Cellular/Molecular

The Origin of Physiological Local mGluR1 Supralinear Ca^{2+} Signals in Cerebellar Purkinje Neurons

Karima Ait Ouares[1,2] **and Marco Canepari**[1,2,3]

[1]University of Grenoble Alpes, CNRS, LIPhy, F-38000 Grenoble, France, [2]Laboratories of Excellence, Ion Channel Science and Therapeutics, France, and [3]Institut National de la Santé et Recherche Médicale, France

In mouse cerebellar Purkinje neurons (PNs), the climbing fiber (CF) input provides a signal to parallel fiber (PF) synapses, triggering PF synaptic plasticity. This signal is given by supralinear Ca^{2+} transients, associated with the CF synaptic potential and colocalized with the PF Ca^{2+} influx, occurring only when PF activity precedes the CF input. Here, we unravel the biophysical determinants of supralinear Ca^{2+} signals associated with paired PF-CF synaptic activity. We used membrane potential (V_m) and Ca^{2+} imaging to investigate the local CF-associated Ca^{2+} influx following a train of PF synaptic potentials in two cases: (1) when the dendritic V_m is hyperpolarized below the resting V_m, and (2) when the dendritic V_m is at rest. We found that supralinear Ca^{2+} signals are mediated by type-1 metabotropic glutamate receptors (mGluR1s) when the CF input is delayed by 100–150 ms from the first PF input in both cases. When the dendrite is hyperpolarized only, however, mGluR1s boost neighboring T-type channels, providing a mechanism for local coincident detection of PF-CF activity. The resulting Ca^{2+} elevation is locally amplified by saturation of endogenous Ca^{2+} buffers produced by the PF-associated Ca^{2+} influx via the mGluR1-mediated nonselective cation conductance. In contrast, when the dendritic V_m is at rest, mGluR1s increase dendritic excitability by inactivating A-type K^+ channels, but this phenomenon is not restricted to the activated PF synapses. Thus, V_m is likely a crucial parameter in determining PF synaptic plasticity, and the occurrence of hyperpolarization episodes is expected to play an important role in motor learning.

Key words: **calcium channels; cerebellar Purkinje neuron; climbing fibre; endogenous calcium buffer; metabotropic glutamate receptors; parallel fibre**

Significance Statement

In Purkinje neurons, parallel fiber synaptic plasticity, determined by coincident activation of the climbing fiber input, underlies cerebellar learning. We unravel the biophysical mechanisms allowing the CF input to produce a local Ca^{2+} signal exclusively at the sites of activated parallel fibers. We show that when the membrane potential is hyperpolarized with respect to the resting membrane potential, type-1 metabotropic glutamate receptors locally enhance Ca^{2+} influx mediated by T-type Ca^{2+} channels, and that this signal is amplified by saturation of endogenous buffer also mediated by the same receptors. The combination of these two mechanisms is therefore capable of producing a Ca^{2+} signal at the activated parallel fiber sites, suggesting a role of Purkinje neuron membrane potential in cerebellar learning.

Introduction

In cerebellar Purkinje neurons (PNs), short-term and long-term synaptic plasticity of the parallel fiber (PF) inputs can be induced by pairing PF EPSPs with a climbing fiber (CF) EPSP (Wang et al., 2000; Brenowitz and Regehr, 2005; Safo and Regehr, 2005). These forms of plasticity, which are believed to underlie associative motor learning and control behaviors (Ito, 2001), are homosynaptic and require local Ca^{2+} elevation at the site of activated PF synapses. Precisely, the Ca^{2+} transient triggered by a CF-EPSP alone is not local (Knöpfel et al., 1991; Miyakawa et al., 1992; Canepari and Vogt, 2008; Ait Ouares et al., 2019) because it is caused by a depolarizing transient, originating in the soma and in the initial dendritic segment, that spreads to distal dendrites to open voltage-gated Ca^{2+} channels (VGCCs). When a CF-EPSP occurs after PF activity, the associated Ca^{2+} transient is larger than the summation of the two Ca^{2+} transients triggered by PF and CF inputs alone and is therefore referred to as "supralinear" Ca^{2+} signal (Brenowitz and Regehr, 2005). However, in contrast to the Ca^{2+} transient associated with an unpaired CF-EPSP, the supra-

Received Oct. 9, 2019; revised Jan. 9, 2020; accepted Jan. 11, 2020.

Author contributions: M.C. designed research; K.A.O. performed research; K.A.O. and M.C. analyzed data; M.C. wrote the paper.

This work was supported by the Agence Nationale de la Recherche through three grants (ANR-14-CE17-0006 – WaveFrontImag; Labex *Ion Channels Science and Therapeutics:* program number ANR-11-LABX-0015; and National Infrastructure France Life Imaging "Noeud Grenoblois") and by the Federation pour la recherché sur le Cerveau (Grant *Espoir en tête*, Rotary France). We thank Dr. Boris Barbour for useful discussions during the project, for reading the manuscript before submission, and for advice on improving the clarity of the figures.

The authors declare no competing financial interests.

Correspondence should be addressed to Marco Canepari at marco.canepari@univ-grenoble-alpes.fr.

https://doi.org/10.1523/JNEUROSCI.2406-19.2020

linear Ca^{2+} signal associated with paired PF and CF inputs is localized exclusively at the site of activated PF synapses.

The ability of a spread physiological signal to trigger a local signal, in combination with synaptic activity, exclusively at the sites of activated synapses is a crucial requirement for coincident detection and associative plasticity in many systems. In hippocampal and neocortical pyramidal neurons, synchronous action potentials and excitatory synaptic activity can potentiate activated synapses (Debanne, 1996). In this case, action potentials transiently depolarizing the dendrites can provide a signal localized at activated synapses by unblocking NMDA receptors from Mg^{2+} (Ascher and Nowak, 1987). However, in the case of PF synaptic plasticity induced by coincident CF inputs, the underlying biophysical mechanism does not involve NMDA receptors but instead type-1 metabotropic glutamate receptors (mGluR1s), which are locally activated by glutamate release from PF terminals (Hartell, 1994; Wang et al., 2000; Brenowitz and Regehr, 2005; Safo and Regehr, 2005). Because mGluR1 activation is not voltage-dependent, the fundamental question is to understand how a CF-EPSP, which alone generates a depolarization and a Ca^{2+} influx everywhere in the dendrite, can trigger a strong localized Ca^{2+} elevation, in combination with mGluR1 activation, exclusively at the site of activated PFs.

In a recent study, we demonstrated that the dendritic depolarization produced by a CF-EPSP activates two types of VGCCs, T-type and P/Q-type VGCCs, and that the activation of both channels is determined by the dendritic membrane potential (V_m) at the beginning of the CF-EPSP (Ait Ouares et al., 2019). Specifically, at initial hyperpolarized V_m, the dendritic Ca^{2+} transient is largely mediated by T-type VGCCs, whereas activation of A-type voltage-gated K^+ channels limits the opening of P/Q-type VGCCs. In contrast, at initial depolarized V_m, T and A channels are inactivated, and the larger dendritic depolarizing transient activates P/Q-type VGCCs that mediate Ca^{2+} spikes. It was also shown that both T-type VGCCs (Hildebrand et al., 2009; Isope et al., 2012) and P/Q-type VGCCs (Otsu et al., 2014) can be boosted by mGluR1 activation, providing two potential biophysical mechanisms underlying localized supralinear Ca^{2+} signals that are required for coincident detection and PF synaptic plasticity.

In the present study, we addressed the question of how a CF-EPSP can generate a supralinear Ca^{2+} signal exclusively at the sites of activated PF synapses. We used a protocol of moderate PF stimulation mimicking a physiological burst to reveal the biophysical mechanism that permits a CF-EPSP to trigger a localized signal at the site of activated PF synapses in realistic scenarios. We used ultrafast V_m and Ca^{2+} imaging, using indicators of different affinity and a series of selective pharmacological manipulations, and we performed a detailed analysis to elucidate the different mechanisms underlying supralinear Ca^{2+} signals under different conditions.

Materials and Methods

Slice preparation, solutions, electrophysiology, and pharmacology

Experiments were ethically performed in accordance with European Directives 2010/63/UE on the care, welfare, and treatment of animals. Procedures were reviewed by the ethics committee affiliated with the animal facility of the university (D3842110001). We used mice aged 21–35 postnatal days (C57BL/6j) of either sex. Animals were anesthetized by isoflurane inhalation, and the entire cerebellum was removed after decapitation. Cerebellar sagittal slices (250 μm thick) were prepared following established procedures (Vogt et al., 2011a,b; Ait Ouares et al., 2016) using a Leica VT1200 (Leica). Slices were incubated at 37°C for 45 min before use. The extracellular solution contained the following (in mM): 125 NaCl, 26 $NaHCO_3$, 1 $MgSO_4$, 3 KCl, 1 NaH_2PO_4, 2 $CaCl_2$, and 20 glucose, bubbled with 95% O_2 and 5% CO_2. The intracellular solution contained the following (in mM): 125 $KMeSO_4$, 5 KCl, 8 $MgSO_4$, 5 Na_2-ATP, 0.3 Tris-GTP, 12 Tris-phosphocreatine, 20 HEPES, adjusted to pH 7.35 with KOH. In V_m imaging experiments, PNs were loaded with the voltage-sensitive dye (VSD) JPW1114 as previously described (Canepari and Vogt, 2008), and in some experiments, PNs were also loaded with the Ca^{2+} indicator Fura-2FF (at 1 mM) using a previously described procedure (Vogt et al., 2011a). In experiments of Ca^{2+} imaging only, Oregon Green BAPTA-5N (OG5N) was added to the internal solution at 2 mM concentration, and in some experiments, Fura-2 (Fura2) at 0.4 mM concentration was also included. Patch-clamp recordings were made at 32°C–34°C using a MultiClamp 700A amplifier (Molecular Devices), and electrical signals were acquired at 20 kHz using the analog-to-digital board of the CCD camera, regardless of the imaging acquisition rate. The measured V_m was corrected for junction potential (−11 mV) as previously estimated (Canepari et al., 2010). PF-EPSPs and CF-EPSPs were elicited by current pulses of 5–20 μA amplitude and 100 μs duration delivered by separate electrodes. To avoid jitters, the stimulation protocols were precisely controlled with a Master-8 pulse generator (A.M.P.I.). All recordings were performed at least 30 min after establishing whole cell. This minimum time before recording started was 45 min in experiments with Fura2, heparin, and ryanodine. In V_m imaging experiments, cells were initially loaded with the voltage-sensitive dye JPW1114 and repatched with a solution without this dye to avoid toxicity due to dye overloading. 7-(Hydroxyimino)cyclopropa[*b*]chromen-1a-carboxylate ethyl ester (CPCCOEt), (1*S*,2*S*)-2-[2-[[3-(1*H*-benzimidazol-2-yl)propyl]methylamino]ethyl]-6-fluoro-1,2,3,4-tetrahydro-1-(1-methylethyl)-2-naphthalenyl-cyclopropanecarboxylate-dihydrochloride (NNC550396 or NNC), and *N*,*N*,*N*-trimethyl-5-[(tricyclo[3.3.1.1^{3,7}]dec-1-ylmethyl)amino]-1-pentanaminium bromide hydrobromide (IEM1460) were dissolved in extracellular solution and applied to the bath via the perfusion system. Heparin sodium salt, 1*H*-pyrrole-2-carboxylic acid (3*S*,4*R*,4a*R*,6*S*,7*S*,8*R*,8a*S*,8b*R*,9*S*,9a*S*)-dodecahydro-4,6,7,8a,8b,9a-hexahydroxy-3,6a,9-trimethyl-7-(1-methylethyl)-6,9-methanobenzo[1,2]pentaleno[1,6-*bc*]furan-8-yl ester (ryanodine), and 1-[6-[[(17β)-3-methoxyestra-1,3,5(10)-trien-17-yl]amino]hexyl]-1*H*-pyrrole-2,5-dione (U73122) were dissolved in intracellular solution and applied via the patch recording. (*S*)-3,5-Dihydroxyphenylglycine (DHPG), dissolved in external solution, was applied through a pipette positioned near the PN dendrite using 20 ms pulses of pressure provided by a pressure ejector, PDES-2DX (npi). AmmTx, dissolved in external solution, was applied through a pipette positioned near the PN dendrite by continuous gentle pressure application. CPCCOEt, heparin sodium salt, ryanodine, U73122, NNC550396, and DHPG were purchased from Tocris Bioscience. IEM1460 was purchased from Hello Bio. AmmTx was purchased from Smartox Biotechnology.

Optical recording

Invitrogen OG5N (Thermo Fisher Scientific) was excited at 470 nm with an OptoLED (Cairn Research) as previously described (Jaafari et al., 2014; Ait Ouares et al., 2016, 2019; Jaafari and Canepari, 2016). Fura-2FF (Santa Cruz Biotechnology) and Invitrogen Fura-2 (Thermo Fisher Scientific) were excited at 385 nm using the OptoLED. V_m and Ca^{2+} optical measurements were achieved sequentially (Canepari and Vogt, 2008) by alternating excitation of Fura-2FF and excitation of the voltage-sensitive dye Invitrogen JPW1114 (Thermo Fisher Scientific) at 528 nm using a LDI laser (89 North). OG5N Ca^{2+} fluorescence was recorded at 530 ± 21 nm. Fura-2FF and Fura2 Ca^{2+} fluorescence was recorded at 510 ± 41 nm. JPW1114 V_m fluorescence was recorded at >610 nm. Image sequences were recorded using a NeuroCCD-SMQ camera (RedShirtImaging). Images were demagnified by ~0.2× to visualize an area of ~150 μm diameter and acquired at 5 or 20 kHz with a resolution of 26 × 26 pixels or 26 × 4 pixels, respectively. In all experiments, four trials, with a 20 s interval between two consecutive trials, were obtained to assess the consistency of the signals and the average of these four trials was used to improve the signal-to-noise ratio. The number of averaged trials was nine in 20 kHz recordings. However, in all figures, the somatic V_m recording used in the illustrations was from a single trial, corresponding to the first trial of the series. Fluorescence was corrected for bleaching using a filtered trial without signal. Ca^{2+} fluorescence transients were expressed as fractional changes of fluorescence ($\Delta F/F_0$), using the average of the first four images of the sequence to calculate F_0. In the color-coded

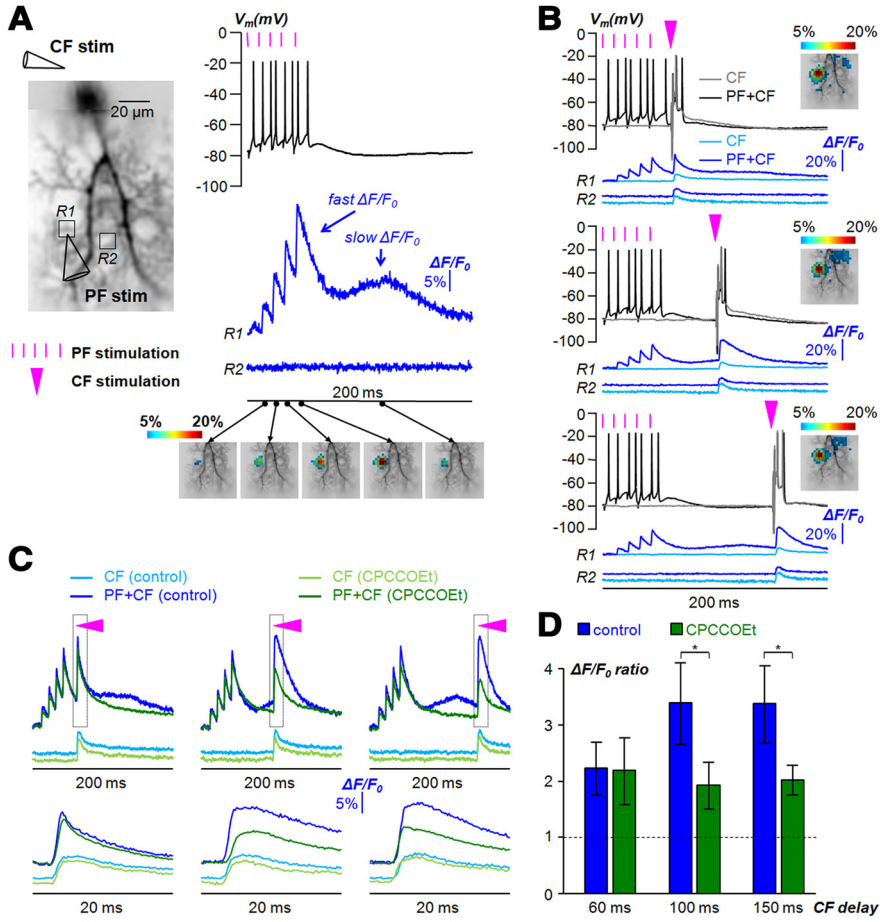

Figure 1. Timing and localization of supralinear Ca^{2+} signals. ***A***, Left, Reconstruction of PN filled with 2 mM OG5N, with position of two stimulating electrodes for the CF and PFs and two regions of interest indicated (*R*1 and *R*2). ***A***, Right, Somatic V_m and Ca^{2+} $\Delta F/F_0$ signals at *R*1 and *R*2 associated with PF stimulation (5 pulses at 100 Hz), with timing indicated by purple lines. Spatial distribution of $\Delta F/F_0$ signal corresponding to the second-fifth PF-EPSPs and to the peak of the slow Ca^{2+} signal depicted using a color code. ***B***, Somatic V_m and Ca^{2+} $\Delta F/F_0$ signals at *R*1 and *R*2 associated with CF stimulation unpaired (light-blue traces) or paired (dark-blue traces) with PF stimulation at 100 Hz (timing indicated by purple lines) following at 60, 100, or 150 ms from the first PF pulse (timing indicated by purple triangles). Spatial distribution of the $\Delta F/F_0$ signal associated with CF-EPSP paired with PF stimulation depicted using a color code. ***C***, Ca^{2+} $\Delta F/F_0$ signals at *R*1 associated with CF stimulation unpaired or paired with PF stimulation delayed by 60, 100, or 150 ms from the first PF pulse in control solution (blue traces) or after addition of 20 μM of the mGluR1 antagonist CPCCOEt (green traces). The time window outlined is reported below. ***D***, Mean ± SD ($N = 6$ cells) of $\Delta F/F_0$ ratio between the paired and unpaired signals in control solution or after addition of CPCCOEt. *Significant inhibition of supralinear Ca^{2+} signal by CPCCOEt ($p < 0.01$, paired *t* test). The dotted line depicts $\Delta F/F_0$ ratio = 1. All optical signals were from averages of four trials.

images, all pixels with intensity value below twice the minimum are set to 1 to exclude pixels with large photon noise threshold, and only those pixels having signal peak >5% are illustrated to appreciate the signal localization. V_m fluorescence transients were calibrated in mV using prolonged hyperpolarizing steps as described in a previous article (Ait Ouares et al., 2019).

Model and computer simulations of calcium binding to the indicators

A simplified version of the model described by Ait Ouares et al. (2016) was used to estimate the Ca^{2+} fluorescence signals in the presence of 2 mM OG5N and 400 μM Fura2. The model consists of a set of equations:

$$\frac{d[Ca^{2+}]}{dt} = \xi_{Ca} - \sum_{j=1}^{4}(K_{ON}^{B_j}\cdot[B_j]\cdot[Ca^{2+}] - K_{OFF}^{B_j}\cdot[B_jCa^{2+}])$$

$$\frac{d[B_jCa^{2+}]}{dt} = K_{ON}^{B_j}\cdot[Ca^{2+}]\cdot[B_j] - K_{OFF}^{B_j}\cdot[B_jCa^{2+}]$$

$$\frac{d[B_j]}{dt} = -\frac{d[B_jCa^{2+}]}{dt}.$$

This model comprises four buffers, with association and dissociation constants K_{ON}^{Bj} and K_{OFF}^{Bj}, respectively. Buffers 1 and 2 are the indicators OG5N and Fura2, respectively, having $K_{ON}^{Fura2} = 570\ \mu M^{-1}\ s^{-1}$ (Canepari and Mammano, 1999) and K_D (K_{OFF}/K_{ON}) = 35 and 0.2 μM, respectively. Buffers 3 and 4 are the two pairs of binding sites of calbindin D-28k, having $K_{ON} = 217.5$ and $27.5\ \mu M^{-1}\ s^{-1}$ and $K_{OFF} = 35.8\ s^{-1}$ nM and $2.6\ s^{-1}$, respectively, as used by Ait Ouares et al. (2019), to account for the difference in temperature and the radial diffusion from the published values (Nägerl et al., 2000). Calbindin D-28k dominates Ca^{2+} binding in the millisecond time scale (Schmidt and Eilers, 2009) and has an estimated concentration of 120 μM (Kosaka et al., 1993). The Ca^{2+} influx associated with the CF was approximated by a Gaussian function of 15 or 20 μM/ms and a 1.5 ms time constant, consistent with the detailed model described by Ait Ouares et al. (2019). We simulated 200 ms of recording using the function "ode45" in MATLAB (MathWorks). In these 200 ms, the Gaussian function approximating the CF-associated Ca^{2+} influx was delayed by 180 ms from the beginning of the simulation, and in the simulations corresponding to the paired scenarios, it was preceded by a slow Ca^{2+} influx approximated by another Gaussian function of 4 μM/ms and a 45 ms time constant to estimate the effect of saturating the high-affinity buffers. The OG5N $\Delta F/F_0$ signal was extrapolated from the Ca^{2+} bound to the indicator using the dynamic range of 15 measured by Ait Ouares et al. (2016). The Fura2 $-\Delta F/F_0$ signal was extrapolated from the Ca^{2+} bound to the indicator using the dynamic range of 0.9 as used by Ait Ouares et al. (2019).

Experimental design and statistical analysis

Data were processed and analyzed using MATLAB. Changes produced by the pairing protocol with respect to the CF stimulation alone, or by the pharmacological action of an agent, were assessed by performing the paired Student's *t* test on the signal parameter under the two different conditions. A change in the signal was considered significant when $p < 0.01$. In all figures, a significant change was indicated with *. In the specific case of data reported in Figure 1, the conclusion that the effect of adding CPCCOEt is different when the CF stimulation is delayed by 60 ms from the first PF stimulus, with respect to the cases of 100 and 150 ms delays, is supported by a paired *t* test performed on the $\Delta F/F_0$ ratios at two different delays that gave a value of $p < 0.01$.

For the quantitative interpretation of the results of combined Ca^{2+} imaging with the low-affinity indicator OG5N and with the high-affinity indicator Fura2, we calculated the variable *S*, defined as follows:

$$S = \begin{cases} \dfrac{\text{paired } \Delta F/F_0(\text{hyp})}{\text{unpaired } \Delta F/F_0(\text{hyp})} & \text{if the initial } V_m \text{ is at hyp state} \\ \dfrac{\text{paired } \Delta F/F_0(\text{rest})}{\text{unpaired } \Delta F/F_0(\text{rest})} & \text{if the initial } V_m \text{ is at rest state} \end{cases}.$$

It must be noticed that *S* is principally used to analyze the supralinear Ca^{2+} signal at the hyperpolarized and resting states, and therefore, both

the numerator and the denominator are different according to the different initial V_m. If a supralinear Ca^{2+} signal occurs when a CF-EPSP is evoked under two different conditions, such as unpaired and paired, then S(OG5N) is obviously positive because a larger free Ca^{2+} concentration implies a larger fraction of Ca^{2+} bound to the low-affinity indicator OG5N. The parameter S(Fura2) can unambiguously discriminate whether a supralinear Ca^{2+} signal is or is not exclusively due to the saturation of Fura2, and whether it is or is not exclusively due to a larger Ca^{2+} influx through the plasma membrane.

Case of supralinear Ca^{2+} signal exclusively due to the saturation of Fura2. In the presence of Fura2, the larger signal under paired conditions can, in principle, be exclusively due to the saturation of the high-affinity indicator by the Ca^{2+} associated with the PF stimulation. Thus, if less free Fura2 is available to buffer the Ca^{2+} entering the cell during the CF-EPSP, more Ca^{2+} will bind to OG5N and less Ca^{2+} will bind to Fura2 under paired conditions, implying that S(Fura2) will be <1. Thus, if S(Fura2) is >1, it unambiguously proves that the supralinear Ca^{2+} signal is not exclusively due to the saturation of Fura2 (i.e., that at least a fraction of Ca^{2+} bound to the low-affinity indicator OG5N originates from Ca^{2+} influx through the plasma membrane).

Case of supralinear Ca^{2+} signal exclusively due to Ca^{2+} influx through the plasma membrane. If the concentration of Fura2 bound to Ca^{2+} associated with the PF stimulation is negligible with respect to the free Fura2 concentration at the time of the CF-EPSP, then the Ca^{2+} transient entering the cell will linearly bind to OG5N and to Fura2, implying that S will have the same value for the two indicators. Thus, if the ratio S(Fura2)/S(OG5N) = 1, then Fura2 is not saturated. Alternatively, if S(Fura2)/S(OG5N) $<$ 1, then at least a fraction of Ca^{2+} bound to the low-affinity indicator OG5N originates from the saturation of Fura2.

In the specific case in which the unpaired Ca^{2+} signal is the same (i.e., when the initial V_m is at the hyperpolarized state and the delay of the CF stimulation is either 60 or 110 ms from the first PF stimulus), the ratio S(Fura2)/S(OG5N) provides a comparative estimate of the Fura2 saturation. Indeed, regardless of the contribution of the Ca^{2+} influx that is different at the two different delays, the more Fura2 is saturated, the smaller S(Fura2) will be and, conversely, the larger S(OG5N) will be. Thus, the smaller S(Fura2)/S(OG5N) is, the larger the contribution of Fura2 saturation will be.

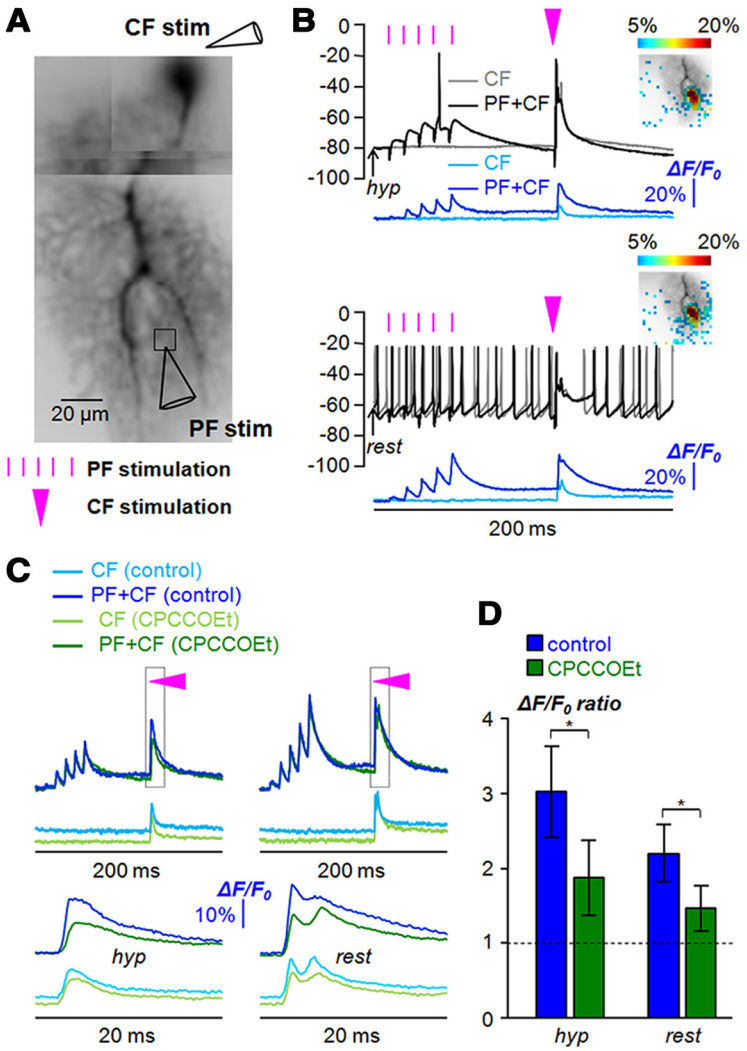

Figure 2. Supralinear Ca^{2+} signals at different initial V_m. ***A***, Reconstruction of PN filled with 2 mM OG5N with the position of two stimulating electrodes for the CF and PFs and a region of interest adjacent to the PF-stimulating electrode indicated. ***B***, Somatic V_m and Ca^{2+} $\Delta F/F_0$ signals at the region of interest associated with CF stimulation unpaired (light-blue traces) or paired (dark-blue traces) with PF stimulation (timing indicated by purple lines) delayed by 110 ms from the first PF pulse (timing indicated by purple triangle) in the case of hyperpolarized (*hyp*; ~−80 mV) or V_{rest} (*rest*; ~−60 mV). Spatial distribution of the $\Delta F/F_0$ signal associated with CF-EPSP paired with PF stimulation depicted using a color code. ***C***, Same Ca^{2+} $\Delta F/F_0$ signals associated with CF stimulation unpaired or paired with PF stimulation in control solution (blue traces) or after addition of 20 μM of the mGluR1 antagonist CPCCOEt (green traces). The time window outlined is reported below. ***D***, Mean ± SD (N = 6 cells) of the $\Delta F/F_0$ ratio between the paired and unpaired signals in control solution or after addition of CPCCOEt. *Significant inhibition of supralinear Ca^{2+} signal by CPCCOEt ($p <$ 0.01, paired t test). The dotted line depicts $\Delta F/F_0$ ratio = 1. All optical signals were from averages of four trials.

Results

Distinct dendritic supralinear Ca^{2+} transients associated with paired PF-CF stimulation

Several studies have shown that, at sites of activated PF synapses, the Ca^{2+} transient associated with a CF-EPSP is significantly larger when it occurs after PF activation (Wang et al., 2000; Brenowitz and Regehr, 2005; Safo and Regehr, 2005; Canepari and Vogt, 2008). To initially analyze these supralinear Ca^{2+} signals, we used a protocol of stimulation for the PF input consisting of five stimuli delivered at 100 Hz with an electrode positioned near a PN dendritic site (Fig. 1*A*), with the initial V_m held between −75 and −85 mV, below the average V_m recorded in the soma when no current is injected (V_{rest}), which was always between −65 and −50 mV. The intensity of stimulation was set to attain a first EPSP in the range of 1–4 mV of somatic amplitude, and the protocol occasionally caused somatic action potentials during the last EPSPs. In cells filled with 2 mM low-affinity Ca^{2+} indicator OG5N (K_D = 35 μM; Canepari and Ogden, 2006), this protocol systematically produced a fast $\Delta F/F_0$ signal, increasing at each individual PF-EPSP, followed by a slow $\Delta F/F_0$ signal peaking at 100–150 ms after the first PF stimulus. As illustrated by the color-coded pictures in Figure 1*A*, both signals were localized within the same area of a few microns adjacent to the PF-stimulating electrode because the sharp depolarization associated with PF-EPSPs is also localized (Canepari and Vogt, 2008). However, at a submicron spatial scale, the two signals are probably not colocalizing, because the fast signal is mediated by VGCCs activated by

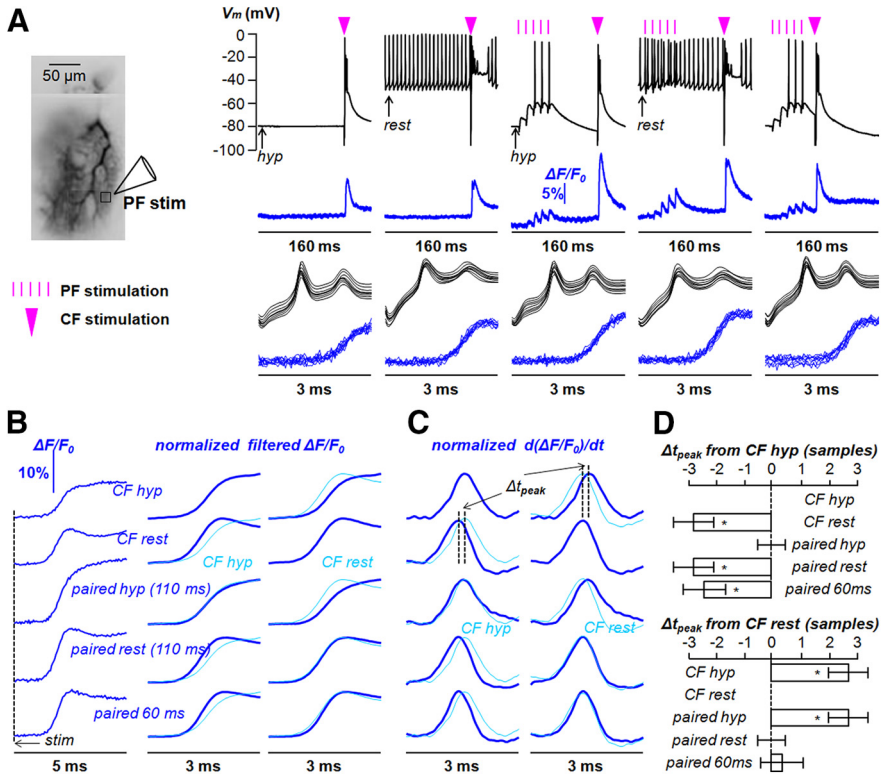

Figure 3. Kinetics of supralinear Ca^{2+} signals. ***A***, Reconstruction of PN filled with 2 mM OG5N; position of PF-stimulating electrode and adjacent region of interest indicated. Somatic V_m and Ca^{2+} $\Delta F/F_0$ signals in the region of interest associated with different protocols: from left to right, a CF-EPSP unpaired at *hyp* and *rest* states, paired with a PF-EPSP train delayed by 110 ms from the first PF stimulus at *hyp* and *rest* states, and paired with a PF-EPSP train delayed by 60 ms from the first PF stimulus. On the bottom, V_m and Ca^{2+} signals associated with the CF-EPSP from the nine individual trials used for the averages aligned and displayed on a 3 ms time window to show that single acquisitions are not affected by jitters. ***B***, Left, Ca^{2+} $\Delta F/F_0$ signals associated with the CF-EPSP reported in ***A*** aligned with the CF stimulation (dotted line indicated by "*stim*") on a time window of 5 ms. ***B***, Right, Same signals smoothed by a 20 point Savitzky–Golay filter and normalized to the peak on a time window of 3 ms. Traces are reported twice, first superimposed to the signal corresponding to the unpaired CF at *hyp* state and second to the signal corresponding to the unpaired CF at *rest* state. ***C***, Normalized time derivative $[d(\Delta F/F_0)/dt]$ of the filtered signals in ***B***. Traces are reported twice, first superimposed to the time derivative corresponding to the unpaired CF at *hyp* state and second to the time derivative corresponding to the unpaired CF at *rest* state. The dotted lines indicate the time of the peak of the $d(\Delta F/F_0)/dt$ signals. Δt_{peak}, Time difference between the two peaks for unpaired CF at *hyp* state and at *rest* state. ***D***, Mean ± SD ($N = 8$ cells) of Δt_{peak} expressed in samples from the signal associated with the unpaired CF at *hyp* state (top) and from the signal associated with the unpaired CF at *rest* state (bottom). *Significant difference from the signal of reference ($p < 0.01$, paired *t* test). All optical signals were from averages of nine trials.

the PF depolarization (Canepari and Vogt, 2008), whereas the slow signal is mediated by a nonselective cation conductance (Canepari et al., 2004), which is believed to be formed by C3-type transient receptor potential (TRPC3) channels (Hartmann et al., 2008).

The time course of the Ca^{2+} transient in the 2 × 2 pixel (~11 × 11 μm^2) region (*R*1) adjacent to the PF-stimulating electrode is reported together with $\Delta F/F_0$ from a control region (*R*2) of the same size, with no Ca^{2+} signal to show the high signal-to-noise ratio of these measurements, permitting a precise quantitative analysis of Ca^{2+} signals. We investigated the Ca^{2+} signal associated with a CF-EPSP unpaired or paired with the PF-EPSPs at delays of 60, 100, or 150 ms from the first PF stimulus (Fig. 1*B*). In all three cases, the Ca^{2+} transient associated with the paired CF-EPSP was larger than that associated with the unpaired CF-EPSP, and these phenomena were restricted to the area where the two Ca^{2+} transients associated with the PF-EPSPs were observed, as illustrated by the color-coded frames in Figure 1*B*. Addition of the mGluR1 inhibitor CPCCOEt (20 μM) reduced the slow $\Delta F/F_0$ signal associated with PF stimulation (Fig. 1*C*) and the supralinear Ca^{2+} signals associated with the CF-EPSP delayed by 100 and 150 ms from the first PF stimulus, but not that associated with the CF-EPSP delayed by 60 ms from the first PF stimulus. In $N = 6$ cells, we quantified the supralinear Ca^{2+} signal by calculating the ratio between the amplitude of the $\Delta F/F_0$ signal associated with the paired CF-EPSP and the amplitude of the $\Delta F/F_0$ signal associated with the unpaired CF-EPSP ($\Delta F/F_0$ ratio; Fig. 1*D*). The $\Delta F/F_0$ ratio significantly ($p < 0.01$, paired *t* test) decreased from 3.40 ± 0.73 to 1.93 ± 0.42 and from 3.38 ± 0.69 to 2.02 ± 0.27 in the cases of 100 and 150 ms delay of the CF stimulation, respectively. In contrast, it did not significantly ($p > 0.1$, paired *t* test) change (from 2.23 ± 0.47 to 2.19 ± 0.60) in the case of 60 ms delay of the CF stimulation. We concluded that supralinear Ca^{2+} signals associated with CF-EPSPs delayed by 100 and 150 ms were mGluR1-dependent, whereas the supralinear Ca^{2+} signal associated with the CF-EPSP delayed by 60 ms was mGluR1-independent.

The CF-associated Ca^{2+} transient at initial hyperpolarized V_m (*hyp*; ~−80 mV) is mainly mediated by Ca^{2+} influx via T-type VGCCs (Ait Ouares et al., 2019). Thus, we further investigated the supralinear Ca^{2+} signal at V_{rest} (*rest*; ~−60 mV); i.e., when T-type VGCCs are mostly inactivated and the CF-associated Ca^{2+} transient is largely mediated by Ca^{2+} influx via P/Q-type VGCCs that can be activated because also most of A-type K^+ channels are inactivated. Again, we used the protocol consisting of five PF stimuli at 100 Hz with an electrode positioned near a PN dendritic site (Fig. 2*A*), followed by a CF-EPSP delayed by 110 ms from the first PF stimulus. In this experiment, however, recordings were performed both at *hyp* and *rest* initial V_m (Fig. 2*B*). In both cases, the Ca^{2+} transient associated with the paired CF-EPSP was larger than that associated with the unpaired CF-EPSP, and both supralinear Ca^{2+} signals were colocalized with the PF active area (see the color-coded frames in Fig. 2*B*). Addition of CPCCOEt reduced both supralinear Ca^{2+} signals associated with the CF-EPSP (Fig. 2*C*). In $N = 6$ cells, the $\Delta F/F_0$ ratio significantly ($p < 0.01$, paired *t* test) decreased from 3.02 ± 0.61 to 1.88 ± 0.50 and from 2.19 ± 0.38 to 1.46 ± 0.30 in the cases of *hyp* and *rest* initial V_m, respectively (Fig. 2*D*). We concluded that supralinear Ca^{2+} signals associated with CF-EPSPs, delayed by 110 ms from the first PF stimulus, were mGluR1-dependent both at *hyp* and at *rest* initial V_m (i.e., independently of whether the CF-associated Ca^{2+} transient is mediated by T-type or P/Q-type VGCCs).

Kinetics of dendritic supralinear Ca^{2+} signals

The three forms of supralinear Ca^{2+} signals presented in the previous paragraph are time-correlated with the CF-associated Ca^{2+} transients, which are mediated by T-type and P/Q-

type VGCCs (Ait Ouares et al., 2019). In principle, they can be due to the modulation of these Ca^{2+} sources, the activation of other Ca^{2+} sources, or both phenomena. If only the original Ca^{2+} source is larger, then the kinetics of the rising phase of the Ca^{2+} transient is expected to be the same for the paired and unpaired CF signal. Thus, useful information can be obtained by analyzing the kinetics of the rising phase of the Ca^{2+} transients in paired protocols with respect to the Ca^{2+} transients associated with unpaired CF-EPSPs, to reveal any possible subsequent component of the Ca^{2+} transients. To this aim, we performed Ca^{2+} recordings associated with the same stimulation protocols described in the previous paragraph, but at 20 kHz in this case to accurately analyze the kinetics of Ca^{2+} transients (Fig. 3*A*). We then analyzed the rising phase of the different Ca^{2+} transients exploiting the short relaxation time of OG5N (Jaafari et al., 2015; Ait Ouares et al., 2016; Jaafari and Canepari, 2016). To quantitatively analyze the fast kinetics of Ca^{2+} transients, we averaged nine recordings for each stimulating protocol (instead of four). As shown in Figure 3*A*, the individual somatic V_m signals and the associated Ca^{2+} transients were perfectly aligned, indicating no jitter in the timing of the CF stimulation. We then normalized the signals to the peak and applied a Savitzky–Golay smoothing filter (Fig. 3*B*) with a 20 point time window, which reduces the noise with minimal distortion of the kinetics of the fluorescence transient (Savitzky and Golay, 1964), as previously demonstrated (Jaafari et al., 2015). Finally, we calculated the time derivative (Jaafari et al., 2014) as shown in Figure 3*C*. The time to peak of the time derivative, from the CF stimulus, is an indirect kinetics measurement of the Ca^{2+} source and is typically longer for T-type VGCCs that principally mediate Ca^{2+} influx at *hyp* states, with respect to P/Q-type VGCCs that principally mediate Ca^{2+} influx at *rest* states (Ait Ouares et al., 2019). Thus, in the example shown in Figure 3*C*, the time difference between the two peaks (Δt_{peak}) at the *hyp* and *rest* states, in the case of unpaired CF-EPSPs, was three samples (150 μs). We then measured the times to peak in the cases of CF-EPSPs in pairing protocol and compared those with the cases of unpaired CF-EPSPs. In the example of Figure 3*C*, the time to peak of the paired CF signal at the *hyp* state was the same as that of unpaired CF signal at the *hyp* state ($\Delta t_{peak} = 0$). In contrast, the times to peak of the paired CF signal at the *rest* state or with the CF stimulation delayed by 60 ms from the first PF stimulus were the same as that of the unpaired CF signal at the *rest* state. We performed this analysis in $N = 8$ cells and calculated Δt_{peak} from the CF signal at both *hyp* (Fig. 3*D*, top) and *rest* states (Fig. 3*D*, bottom). The time to peak of the paired CF signal at *hyp* state was the same as the unpaired CF signal at *hyp* state, and the time to peak of the paired CF signal at *rest* state was the same as the unpaired CF signal at *rest* state. In contrast, the time to peak of the CF signals (paired and unpaired) at *hyp* state was significantly ($p < 0.01$, paired *t* test) longer (by 2.75 ± 0.71 samples) than the time to peak of the CF signals (paired and unpaired) at *rest* state. Finally, the time to peak of the CF signals at *hyp* state was significantly ($p < 0.01$, paired *t* test) longer (by 2.38 ± 0.75 samples) than the time to peak of the paired CF signals with the CF stimulation delayed by 60 ms from the first PF stimulus. Therefore, we concluded that the fast kinetics of Ca^{2+} transients associated with the CF-EPSP are identical in paired and unpaired conditions, both at *hyp* and *rest* states, when the CF stimulation is delayed by 110 ms from the first PF stimulus. This conclusion suggests that the principal Ca^{2+} source of the supralinear Ca^{2+} signal with the CF stimulation delayed by 110 ms from the first PF stimulus at *hyp* states is the T-type VGCC. In contrast, the principal Ca^{2+} source of the supralinear Ca^{2+} signals with the CF stimulation delayed by 110 ms from the first PF stimulus at *rest* states, or with the CF

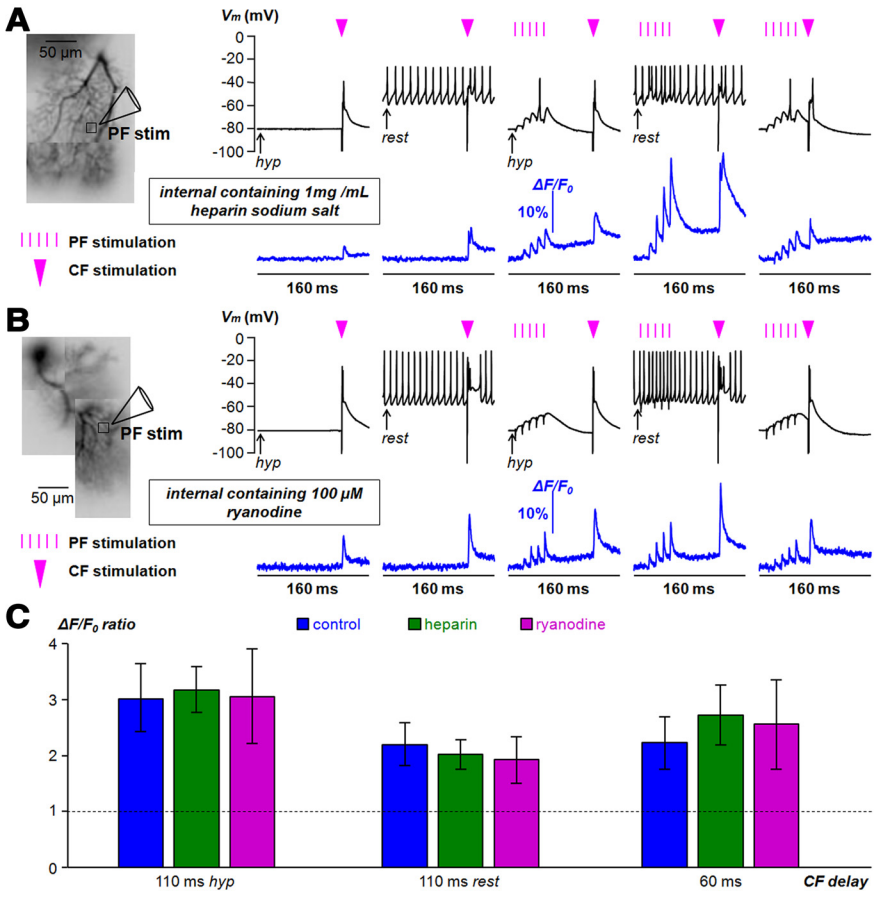

Figure 4. Supralinear Ca^{2+} signals in the presence of heparin or ryanodine. ***A***, Left, Reconstruction of PN filled with 2 mM OG5N and 1 mg/ml of heparin sodium salt to block InsP3 receptors; position of PF-stimulating electrode and adjacent region of interest indicated. Somatic V_m and Ca^{2+} $\Delta F/F_0$ signals in the region of interest associated with different protocols: from left to right, a CF-EPSP unpaired at *hyp* and *rest* states, paired with a PF-EPSP train delayed by 110 ms from the first PF stimulus at *hyp* and *rest* states, and paired with a PF-EPSPs train delayed by 60 ms from the first PF stimulus. ***B***, Same as ***A***, but with the internal solution containing 100 μM ryanodine to block ryanodine receptors. ***C***, Mean ± SD ($N = 6$ cells for each group) of $\Delta F/F_0$ ratio between the paired and unpaired signals in the presence of heparin (green columns) or ryanodine (purple columns). Blue columns are mean ± SD of $\Delta F/F_0$ ratios in control conditions already reported in Figures 1 and 2. Values for heparin were as follows: 3.17 ± 0.41 for 110 ms CF delay at *hyp* states, 2.02 ± 0.27 for 110 ms CF delay at *rest* states, 2.72 ± 0.54 for 60 ms CF delay. Values for ryanodine were as follows: 3.06 ± 0.85 for 110 ms CF delay at *hyp* states, 1.93 ± 0.56 for 110 ms CF delay at *rest* states, 2.56 ± 0.80 for 60 ms CF delay. Experiments were performed 45 min after whole cell to obtain full equilibration of the internal solution. Used concentrations of heparin and ryanodine were the maximal tolerated by the cells for 1 h recording. All optical signals were from averages of four trials.

stimulation delayed by 60 ms from the first PF stimulus, is likely the P/Q-type VGCC.

Yet, several studies have linked PF-triggered activation of mGluR1s to Ca^{2+} release from internal stores, in particular via inositol trisphosphate (InsP3) receptors (Finch and Augustine, 1998; Takechi et al., 1998). To directly test whether Ca^{2+} release from internal stores plays a role in these supralinear Ca^{2+} signals, we performed experiments with the internal solution containing either 1 mg/ml of heparin (Fig. 4*A*) to inhibit Ca^{2+} store release via InsP3 receptors (Kim et al., 2008) or 100 μM ryanodine (Fig. 4*B*) to inhibit Ca^{2+} store release via ryanodine receptors (Kano et al., 1995). In groups of six cells tested with each pharmacological agent, mGluR1-dependent supralinear Ca^{2+} transients were consistent with those measured in control internal solution (Fig. 4*C*). The same result was obtained in a group of six cells, tested at *hyp* states only, injected with 10 μM phospholipase C inhibitor U73122 (data not shown), which was proven to prevent mGluR1-mediated Ca^{2+} release from stores in PN dendrites (Canepari and Ogden, 2006). Together, these results rule out any significant contribution of Ca^{2+} release from stores via either InsP3 or ryanodine receptors.

Dendritic V_m associated with mGluR1-dependent supralinear Ca^{2+} signals

Because Ca^{2+} release from internal stores does not contribute to the supralinear Ca^{2+} signals reported above, the origin of these phenomena can be an increase in the Ca^{2+} influx through the plasma membrane during the CF-EPSP, an increase in free Ca^{2+} concentration (and, therefore, in the Ca^{2+} bound to the OG5N) due to a transient saturation of endogenous Ca^{2+} buffers, or a combination of both phenomena. If the supralinear Ca^{2+} signal includes an increase of Ca^{2+} influx through the plasma membrane, the additional charge influx is expected to increase the electrical current and, therefore, the dendritic V_m transient associated with the CF-EPSP. We initially measured dendritic V_m associated with a paired CF-EPSP delayed by 60 ms from the first PF stimulus using V_m imaging from a region adjacent to the PF stimulation electrode. V_m fluorescence transients were calibrated on an absolute scale (in mV) using prolonged hyperpolarizing pulses as previously described (Canepari and Vogt, 2008; Ait Ouares et al., 2019) to quantify the depolarization associated with the CF-EPSP under different conditions. In the experiment reported in Figure 5*A*, the initial V_m before the CF-EPSP shifted from −80 to −62 mV when the PF-EPSP train was applied (Fig. 5*B*). Consistent with the fact that at this initial V_m, A-type K^+ channels are partially inactivated, and activation of P/Q-type VGCCs is boosted (Ait Ouares et al., 2019), the peak V_m shifted from −21 to −3 mV. Significant shifts in the initial and peak V_m were observed in $N = 8$ cells in which this experiment was performed (Fig. 5*C*), confirming that the mGluR1-independent supralinear Ca^{2+} signal, occurring when the CF-EPSP is at the end of the PF-EPSP train, is associated with a shift from T-type VGCCs to P/Q-type VGCCs, as suggested by the results reported in Figure 3.

After this first set of V_m experiments, we performed combined V_m and Ca^{2+} imaging recordings with a similar approach recently used to characterize the dendritic V_m transient associated with the unpaired CF-EPSP (Ait Ouares et al., 2019) to measure dendritic V_m associated with mGluR1-dependent supralinear Ca^{2+} signals. The cell shown in Figure 6*A* was filled with the VSD JPW1114 and with 1 mM low-affinity Ca^{2+} indicator Fura-2FF ($K_D = 6$ μM; Hyrc et al., 2000), used to localize the area of supralinear Ca^{2+} signals both at *hyp* and *rest* initial V_m (Fig. 6*A*).

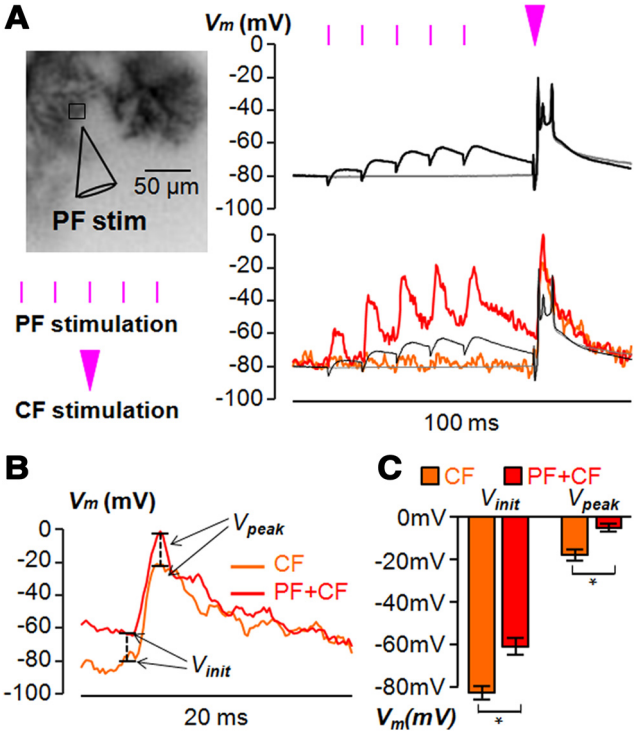

Figure 5. Dendritic V_m associated with mGluR1-independent supralinear Ca^{2+} signals. ***A***, Left, Dendrite of PN filled with the voltage-sensitive dye JPW1114; position of PF-stimulating electrode and adjacent region of interest indicated. ***A***, Right, Somatic (top) and dendritic (bottom) V_m in the region of interest associated with a CF-EPSP unpaired or paired with a PF-EPSP train, with the CF stimulation delayed by 60 ms from the first PF stimulus. ***B***, In a time window of 20 ms, dendritic V_m signals of ***A***. V_{init} and V_{peak}, Initial and peak V_m, respectively, calibrated in mV. ***C***, Mean ± SD ($N = 8$ cells) of V_{init} and V_{peak} for the signals associated with an unpaired CF-EPSP (−83 ± 3 and −18 ± 5 mV, respectively) and for the signals associated with a CF-EPSP paired with a PF-EPSP train, with the CF stimulation delayed by 60 ms from the first PF stimulus (−61 ± 4 and −5 ± 2 mV, respectively). *Significant differences of V_{init} and V_{peak} ($p < 0.01$, paired *t* test). All optical signals were from averages of four trials.

Consistent with the observation that PF-ESPSs locally activate VGCCs at *hyp* initial V_m, the depolarization associated with the PF train was >−30 mV in the region (*R*1) adjacent to the stimulating electrode, whereas the depolarization was comparable with that in the soma in a different region (*R*2), as shown in Figure 6*B*. To excite VSD fluorescence >160 ms without causing photodamage, we used only 20% of the laser intensity applied for previous CF-associated V_m measurements (Ait Ouares et al., 2019). Using this weaker illumination, the SD of the photon noise was equivalent to ~2.5 mV after calibration, and the peak-to-peak noise was equivalent to ~10 mV in *R*1 (Fig. 6*B*). Therefore, to allow discrimination of V_m changes of <3 mV, we applied the following filtering procedures (Fig. 6*C*). For the unpaired CF recordings, the initial V_m was set to the averaged V_m signal before CF stimulation. For the paired CF recordings, the initial V_m was accurately estimated by applying a 64-point median filter to the original fluorescence signal after the end of the PF stimulation. Finally, for all recordings, a 4-point median filter was applied to the 20 ms fluorescence signal following CF stimulation. Figure 6*D* shows a small but detectable additional depolarization associated with the paired CF-EPSP at both *hyp* and *rest* initial V_m. In $N = 7$ cells, in which we successfully combined V_m and Ca^{2+} with filtered signals above the photon noise to discriminate V_m changes <3 mV, the additional depolarization, calculated as the difference between the paired and unpaired CF-associated V_m transients, was always detectable in the case of *hyp* initial V_m and

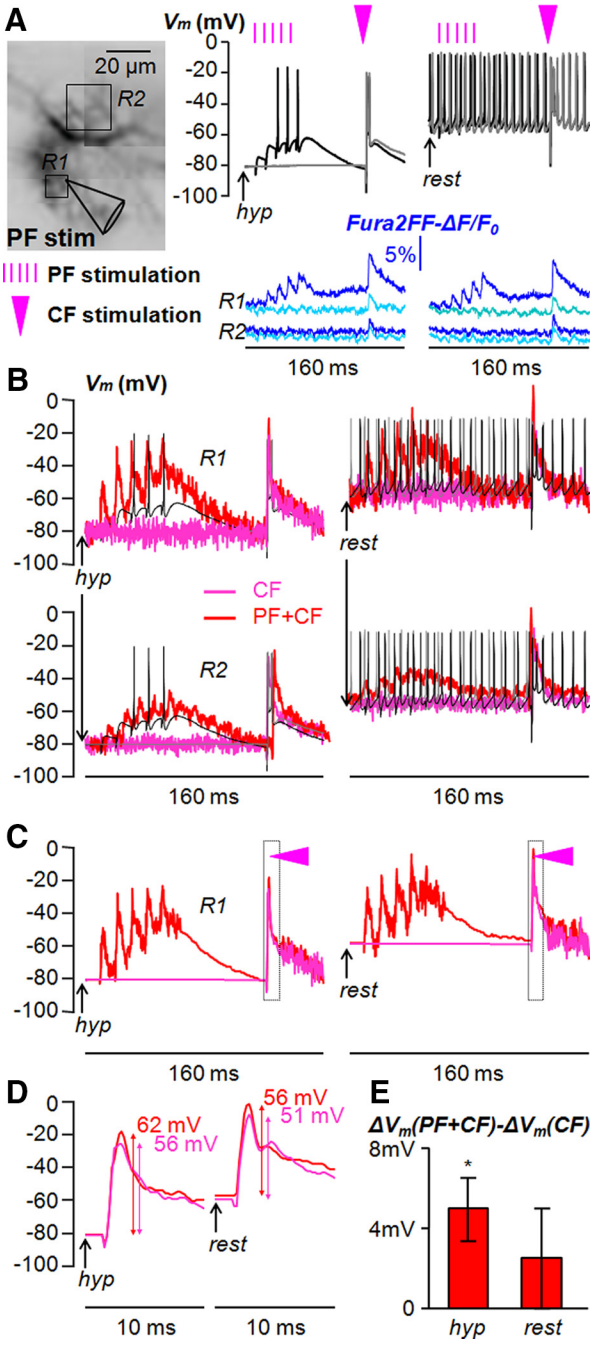

Figure 6. Dendritic V_m transients associated with mGluR1-dependent supralinear Ca^{2+} signals. ***A***, Left, Dendritic PN area filled with the VSD JPW1114 and 1 mM Fura-2FF; position of PF-stimulating electrode and two regions of interest (*R*1 and *R*2) indicated. ***A***, Right, Somatic V_m and Fura-2FF $-\Delta F/F_0$ signals from single trials at *R*1 and *R*2 associated with CF stimulation unpaired (light-blue traces) or paired (dark-blue traces) with PF stimulation in the case of *hyp* (~−80 mV) or *rest* (~−60 mV) initial V_m, indicating supralinear Ca^{2+} signals at *R*1. ***B***, V_m-calibrated recordings associated with CF stimulation unpaired (red traces) or paired (pink traces) with PF stimulation at *R*1 and *R*2 superimposed to somatic V_m, in the case of *hyp* or *rest* initial V_m. ***C***, V_m recordings at *R*1 shown in ***B*** filtered as follows: for the unpaired CF, the average of the signals before the CF stimulation is used and in the next 20 ms a 4-points median filter is applied; for the paired CF, a 64-point median filter is applied after the PF train and before the CF stimulation, and a 4-point median filter is applied in the next 20 ms. ***D***, Same signals as ***C*** in the outlined time window; the values of the V_m transients are indicated. ***E***, Mean ± SD ($N = 7$ cells) of the V_m transient difference between the paired and unpaired CF in the case of *hyp* or *rest* initial V_m. *Significant difference ($p < 0.01$, paired *t* test). All optical signals were from averages of four trials.

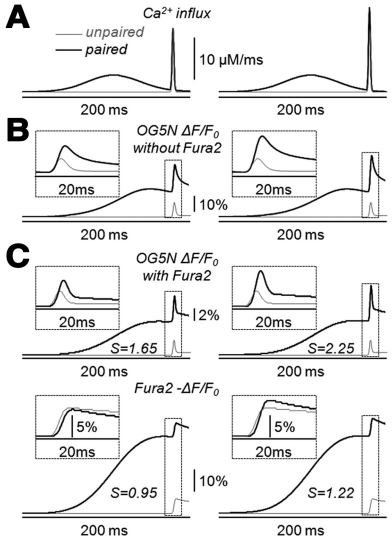

Figure 7. Computer simulations of the Ca^{2+} fluorescence signals in the presence of 2 mM OG5N and 400 µM Fura-2. ***A***, Left, Right, Ca^{2+} influx used in the computer simulations associated with a CF-EPSP: Gaussian function of 15 µM/ms (left) or 20 µM/ms (right) and 1.5 ms time constant unpaired or paired with a preceding slow Ca^{2+} influx approximated by another Gaussian function of 4 µM/ms and 45 ms time constant. ***B***, Computer simulations of the putative OG5N $\Delta F/F_0$ signal in the absence of Fura2 using the model described in detail in the Materials and Methods and the Ca^{2+} influx reported in ***A***. The $\Delta F/F_0$ signal was extrapolated from the Ca^{2+} bound to the indicator using the dynamic range of 15 measured by Ait Ouares et al. (2016). ***C***, Top, Bottom, Computer simulations of the putative OG5N $\Delta F/F_0$ signal (top) and the putative Fura2 $-\Delta F/F_0$ signal (bottom) in the presence of 400 µM Fura2 using the same model and Ca^{2+} influx as in ***B***. The Fura2 $-\Delta F/F_0$ signal was extrapolated from the Ca^{2+} bound to the indicator using the dynamic range of 0.9 used by Ait Ouares et al. (2019). The values of the variable *S*, described in detail in the Experimental design and statistical analysis section of the Materials and Methods, are reported for the two indicators.

corresponded to a significant increase of 5.0 ± 1.6 mV ($p < 0.01$, paired *t* test). In the case of *rest* initial V_m, a detectable increase (>3 mV) was observed only in four of seven cells. The mean ± SD of the V_m was 2.5 ± 2.5 mV ($N = 7$ cells). We concluded that small additional V_m transients are always associated with mGluR1-dependent supralinear Ca^{2+} signals at *hyp* initial V_m, a result consistent with the hypothesis that at least part of the supralinear Ca^{2+} signal under this condition is due to Ca^{2+} influx through the plasma membrane. In the case of *rest* initial V_m, additional V_m transients were occasionally observed, suggesting a smaller and possibly highly variable contribution of Ca^{2+} influx through the plasma membrane.

Contribution of the saturation of the endogenous buffer to the supralinear Ca^{2+} signals

In a previous study, we have shown that trains of PF stimuli at 100 Hz produce a local progressive saturation of endogenous Ca^{2+} buffers that boosts a Ca^{2+} fluorescent transient associated with a CF-EPSP occurring at the end of the PF train (Canepari and Vogt, 2008). Because mGluR1 activation induces a slow Ca^{2+} influx, saturation of the endogenous Ca^{2+} buffer may occur on a longer time scale and contribute to the mGluR1-dependent supralinear Ca^{2+} signals. To test whether this phenomenon occurs, experiments can be performed with the inclusion of the high-affinity UV-excitable indicator Fura2 (K_D ~200 nM). We initially tested different Fura2 concentrations (100, 200, and 400 µM), and we finally chose the concentration of 400 µM because, under this condition, the Fura2 signal was not saturated by a CF Ca^{2+} transient, and the OG5N was still large enough to be accurately ana-

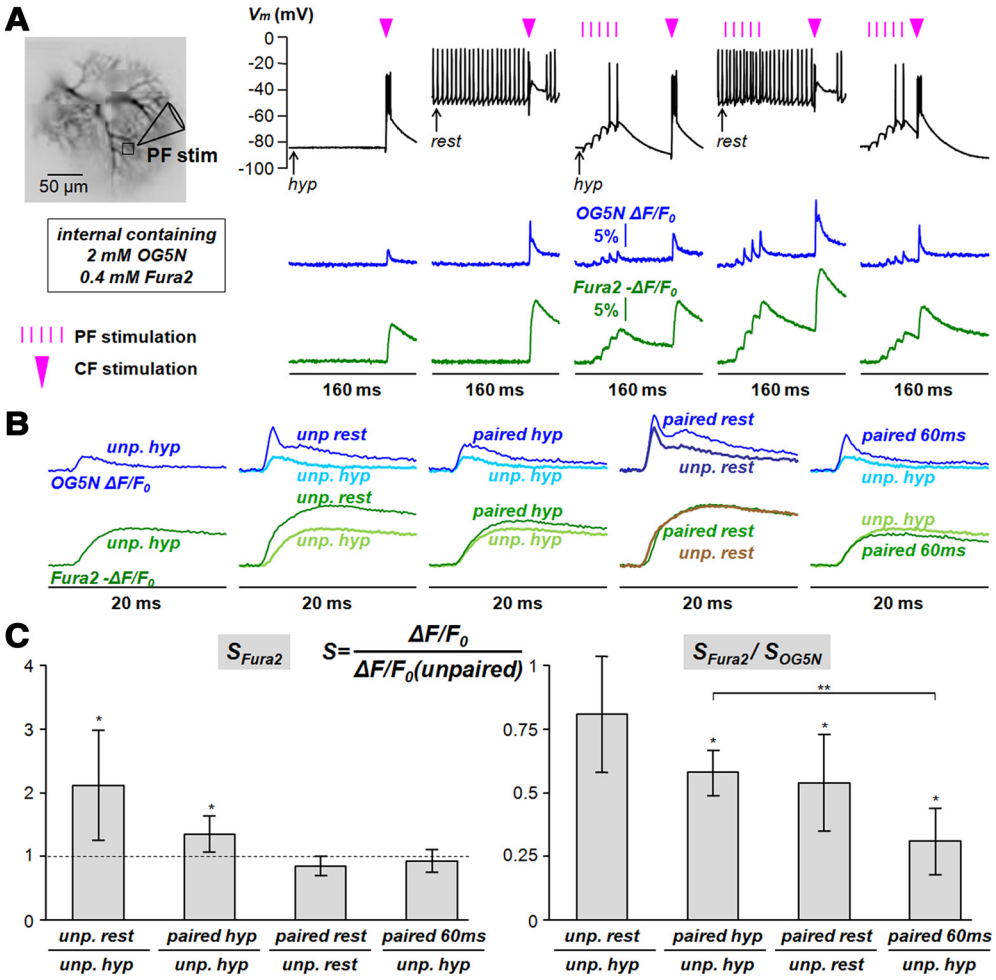

Figure 8. Contribution of saturation of endogenous Ca^{2+} buffers to supralinear Ca^{2+} signals. ***A***, Left, Dendritic PN area filled with two Ca^{2+} indicators: OG5N (2 mM, $K_D = 35\ \mu M$) and Fura2 (0.4 mM, $K_D = 0.2\ \mu M$); position of PF-stimulating electrode and adjacent region of interest are indicated. Somatic V_m and Ca^{2+} signals in the region of interest associated with different protocols: from left to right, a CF-EPSP unpaired at *hyp* and *rest* states, paired with a PF-EPSP train delayed by 110 ms from the first PF stimulus at *hyp* and *rest* states, and paired with a PF-EPSP train delayed by 60 ms from the first PF stimulus; signals from the two indicators (OG5N $\Delta F/F_0$ and Fura $-\Delta F/F_0$) were obtained by alternating the excitation wavelength. ***B***, Same Ca^{2+} transients associated with the CF-EPSP in ***A***, for the two indicators, superimposed either to the unpaired CF transient at *hyp* state or to the unpaired CF transient at *rest* state. ***C***, *S* is defined as the ratio between the $\Delta F/F_0$ peaks for each protocol and the $\Delta F/F_0$ peak associated with the unpaired CF stimulation. ***C***, Left, Mean ± SD ($N = 8$ cells) of *S* corresponding to Fura2 signals (S_{Fura2}) in the different cases as reported in the legend. *Significant difference ($p < 0.01$, paired *t* test) between the two $\Delta F/F_0$ peaks used to calculate S_{Fura2}. ***C***, Right, Mean ± SD ($N = 8$ cells) of S_{Fura2}/S_{OG5N} in the different cases as reported in the legend. *Significant difference ($p < 0.01$, paired *t* test) between S_{OG5N} and S_{Fura2}; **significant difference ($p < 0.01$, paired *t* test) between two S_{OG5N}/S_{Fura2} ratios. All optical signals were from averages of four trials.

lyzed. To examine quantitatively how this type of measurement can provide an answer to the question on whether and to what extent the saturation of the endogenous buffer contributes to the supralinear Ca^{2+} signals, we ran computer simulations using the simple but realistic biochemical model described in the Materials and Methods. Specifically, we analyzed a scenario in which the same Ca^{2+} influx associated with a CF-EPSP occurs unpaired or paired with a previous slow Ca^{2+} influx, and another scenario in which the paired Ca^{2+} influx is 25% larger with respect to the unpaired Ca^{2+} influx (Fig. 7*A*). When the simulation is run without Fura2, the putative OG5N $\Delta F/F_0$ exhibits supralinear Ca^{2+} signals under paired conditions in both scenarios (Fig. 7*B*). When the simulation is instead run with Fura2, while supralinear Ca^{2+} signals under paired conditions are still present in the putative OG5N $\Delta F/F_0$, the putative Fura2 $-\Delta F/F_0$ behaves differently in the two scenarios: it exhibits a small supralinear Ca^{2+} signal in the case of potentiated Ca^{2+} influx, but the paired Ca^{2+} signal is smaller than the unpaired Ca^{2+} signal when Ca^{2+} influx is the same (Fig. 7*C*). To quantitatively analyze this result, we introduce the variable *S*, defined as the ratio of the paired $\Delta F/F_0$ peak against the unpaired $\Delta F/F_0$ peak. The conclusive information that can be obtained, by the analysis of the variable *S*, is explained in detail in the Experimental design and statistical analysis section of the Materials and Methods. In brief, when the supralinear Ca^{2+} signal is exclusively due to buffer saturation, then the value of *S* for Fura2 (S_{Fura2}) must be <1 ($S_{Fura2} = 0.95$ in the case of the simulation in Fig. 7*C*). In contrast, a value of $S_{Fura2} > 1$ indicates that larger Ca^{2+} influx contributes to the supralinear Ca^{2+} signal ($S_{Fura2} = 1.22$ in the case of the simulation in Fig. 7*C*). Because a supralinear Ca^{2+} signal exclusively due to larger Ca^{2+} influx (i.e., no buffer saturation) leads to an increase in the absolute $\Delta F/F_0$ signal, which is the same for the two indicators, the ratio of *S* for the two indicators (S_{Fura2}/S_{OG5N}) must be 1 in this case. It follows that a lower value of this ratio indicates that buffer saturation contributes to the supralinear Ca^{2+} signal ($S_{Fura2}/S_{OG5N} = 0.54$ in the case of the simulation in Fig. 7*C*). Thus, S_{Fura2}/S_{OG5N} also represents a quantitative estimate of the extent of buffer saturation in the two cases. With the premise that the analysis of the

saturation of Fura2 provides an estimate for the saturation of the endogenous buffer occurring physiologically, we run experiments by adding 400 μM Fura2 in the patch electrode. In the cell shown in Figure 8*A*, we applied the same stimulation protocols of Figure 3 and measured separately the absolute fluorescent transients from the two indicators (OG5N $\Delta F/F_0$ and Fura2 $-\Delta F/F_0$). Under this condition, supralinear OG5N Ca^{2+} signals were observed (Fig. 8*B*), indicating that these signals are not prevented by the presence of Fura2 at this moderate concentration. In contrast, whereas a supralinear Fura2 Ca^{2+} signal associated with the paired CF-EPSP delayed by 110 ms at the *hyp* state was observed, the Fura2 Ca^{2+} signal associated with the paired CF-EPSP delayed by 60 ms was smaller than the Ca^{2+} signal associated with the unpaired CF-EPSP (Fig. 8*B*). We then calculated the variable S for the ratios of the $\Delta F/F_0$ peaks in each protocol against the $\Delta F/F_0$ peak associated with the unpaired CF stimulation (Fig. 8*C*). In $N = 8$ cells tested, S_{Fura2} was significantly positive for the mGluR1-dependent supralinear Ca^{2+} signal at *hyp* states ($p < 0.01$, paired t test, $S_{Fura2} = 2.38 \pm 0.05$), confirming that larger Ca^{2+} influx through the plasma membrane contributes in this case (Fig. 8*C*). However, S_{Fura2} was significantly smaller than S_{OG5N} ($p < 0.01$, paired t test, $S_{Fura2}/S_{OG5N} = 0.58 \pm 0.09$), indicating that buffer saturation also contributes to this supralinear Ca^{2+} signal. Finally, S_{Fura2}/S_{OG5N} for the mGluR1-independent supralinear Ca^{2+} signal (0.31 ± 0.13) was significantly smaller than S_{Fura2}/S_{OG5N} for the mGluR1-dependent supralinear Ca^{2+} signal ($p < 0.01$, paired t test), indicating that, in this case, buffer saturation provides a larger contribution. The Ca^{2+} increase through P/Q-type VGCCs produced by switching from *hyp* states to *rest* states is essentially due to larger Ca^{2+} influx ($S_{Fura2}/S_{OG5N} = 0.80 \pm 0.23$). Thus, as expected, the further mGluR1-dependent Ca^{2+} increase includes a significant contribution of buffer saturation ($S_{Fura2}/S_{OG5N} = 0.54 \pm 0.19$, calculated using the unpaired CF signal at *rest* state). This analysis, however, does not allow estimating a possible contribution of larger Ca^{2+} influx in the case of mGluR1-dependent supralinear Ca^{2+} signal at *rest* states.

Origin of the mGluR1-dependent supralinear Ca^{2+} signals at initial hyperpolarized V_m

The previously presented results demonstrate that mGluR-dependent supralinear Ca^{2+} signals at the *hyp* state are due to a combination of Ca^{2+} influx increase through the plasma membrane and a transient saturation of the endogenous Ca^{2+} buffer. The rising phase of the paired CF Ca^{2+} signal has the same kinetics as the Ca^{2+} signal associated with the unpaired CF input (Fig. 3), which is principally mediated by T-type VGCCs (Ait Ouares et al., 2019). It has been reported that mGluR1 activation potentiates Cav3.1 T-type VGCCs in PNs (Hildebrand et al., 2009). Hence, we finally assessed directly whether the Ca^{2+} influx component of the mGluR1-dependent supralinear Ca^{2+} signal at *hyp* states is through these channels. In the cell reported in Figure 9*A*, we recorded the Ca^{2+} transient associated with a CF-EPSP unpaired or paired with PF stimulation at *hyp* or *rest* initial V_m in control conditions with a delay of 110 ms from the first PF stimulus and the CF stimulation. Addition of 30 μM of the Cav3.1 blocker NNC550396 inhibited spontaneous firing at *rest* initial V_m and strongly reduced Ca^{2+} transients associated with both PF-EPSPs and the CF-EPSP at *hyp* initial V_m (Fig. 9*A*). In contrast, Ca^{2+} transients associated with both PF-EPSPs and the CF-EPSP at *rest* initial V_m were only slightly affected by NNC addition, confirming that dendritic T-type VGCCs are mostly inactivated at this state (Fig. 9*A*). As shown in Figure 9*B*, the

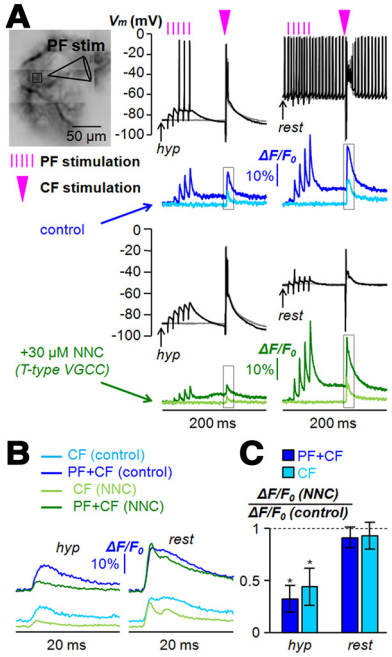

Figure 9. Supralinear Ca^{2+} signals after blocking T-type VGCCs. ***A***, Left, Dendritic area of a PN filled with 2 mM OG5N, with position of PF-stimulating electrode and an adjacent region of interest indicated. ***A***, Right, Somatic V_m (black traces) and Ca^{2+} $\Delta F/F_0$ (blue or green traces) signals at the region of interest associated with CF stimulation unpaired (light traces) or paired (dark traces) with PF stimulation (timing indicated by purple lines) delayed by 110 ms from the first PF pulse (timing indicated by purple triangle) in the case of *hyp* or *rest* initial V_m. Signals were acquired in control conditions (blue traces) or after addition of 30 μM of the T-type VGCC blocker NNC (green traces). ***B***, Same Ca^{2+} signals as in ***A*** over a 20 ms time window. ***C***, Mean ± SD ($N = 6$ cells) of the ratios between the $\Delta F/F_0$ peak after addition of NNC and the peak under control conditions; dark-blue columns are for paired signals; light-blue columns are for unpaired CF signals. Ratios are calculated both for unpaired and paired CF signals. *Significant reduction of paired Ca^{2+} signal after addition of NNC ($p < 0.01$, paired t test). The dotted line depicts ratio = 1. All optical signals were from averages of four trials.

supralinear Ca^{2+} transient at *hyp* initial V_m was also strongly inhibited by addition of NNC. In $N = 6$ cells tested with this experimental protocol, the ratios between the CF Ca^{2+} signals in the presence of NNC and in control condition at initial hyperpolarized V_m were 0.44 ± 0.18 and 0.32 ± 0.13 for the CF unpaired or paired with PF stimulation, respectively (Fig. 9*C*). In both cases, the Ca^{2+} signal associated with the paired CF-EPSP was significantly smaller ($p < 0.01$, paired t test). In contrast, the ratios between the CF Ca^{2+} signals in the presence of NNC and in control condition at *rest* initial V_m were 0.93 ± 0.13 and 0.91 ± 0.10 for the CF unpaired or paired with PF stimulation, respectively, indicating that, in this state, T-type VGCCs contribute marginally to Ca^{2+} signals (Fig. 9*C*). The results reported in Figure 9 unambiguously confirm that the Ca^{2+} influx component responsible for mGluR1-dependent supralinear Ca^{2+} signals at *hyp* state is mediated by T-type Ca^{2+} channels.

As shown in the example of Figure 9*A*, addition of NNC reduced the fast Ca^{2+} transient associated with the PF-EPSP train, whereas it did not affect the slow Ca^{2+} transient mediated by mGluR1s. Furthermore, although both unpaired and paired Ca^{2+} transients were inhibited by NNC, the paired Ca^{2+} transient was still larger (Fig. 9*A*), suggesting that local amplification of the residual component by buffer saturation is still present when T-type VGCCs are blocked. Thus, endogenous buffer is likely saturated by the slow mGluR1-mediated Ca^{2+} influx. To test this hypothesis, we measured mGluR1-dependent supralin-

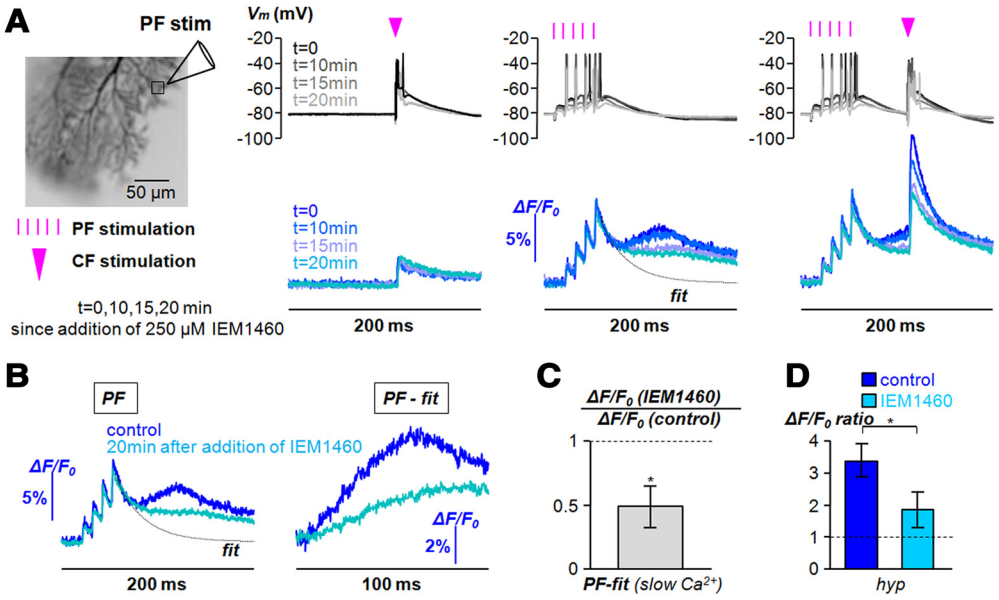

Figure 10. Use-dependent block of mGluR1 slow Ca^{2+} transients and of supralinear Ca^{2+} signals. ***A***, Left, Dendritic area of a PN filled with 2 mM OG5N, with position of PF-stimulating electrode and an adjacent region of interest indicated. Somatic V_m and Ca^{2+} $\Delta F/F_0$ signals at the region of interest associated with an unpaired CF-EPSP, with PFs stimulated with five pulses at 100 Hz or with a CF-EPSP paired with PF stimulation at *hyp* state. Black and dark-blue traces were from recordings in control solution. Traces at different gray or blue tones were from recordings performed a time (*t*) after addition of 250 μM of the channel blocker IEM1460. ***B***, Left, Same recordings as in ***A*** for PF stimulation only (*PF*) in control condition and 20 min after addition of IEM1460; the exponential *fit* of the Ca^{2+} $\Delta F/F_0$ decay after the fifth PF-EPSP is also reported with a dotted line. ***B***, Right, Ca^{2+} transients associated with the slow mGluR1-mediated component calculated as the difference between the Ca^{2+} $\Delta F/F_0$ signals associated with PF stimulation and the *fit* trace on the left. ***C***, Mean ± SD ($N = 6$ cells) of the ratio between the slow mGluR1-dependent PF-mediated Ca^{2+} transients (*PF-fit*) 20 min after addition of IEM1460 and in control condition. *Significant reduction of the signal ($p < 0.01$, paired *t* test). The dotted line depicts ratio = 1. ***D***, Mean ± SD of the $\Delta F/F_0$ ratio between the paired and unpaired signals in control solution or after addition of IEM1460. *Significant inhibition of supralinear Ca^{2+} signal by IEM1460 ($p < 0.01$, paired *t* test). The dotted line depicts $\Delta F/F_0$ ratio = 1. All optical signals were from averages of four trials.

ear Ca^{2+} signals at *hyp* states while blocking the slow mGluR1-mediated Ca^{2+} transient with the channel blocker IEM1460 that does not affect the mGluR1-dependent boosting of T-type VGCCs (Hildebrand et al., 2009). In the example in Figure 10*A*, addition of 250 μM IEM1460 produced a use-dependent block of the slow mGluR1-dependent Ca^{2+} transient over a period of 20 min, in which stimulation protocols were repeated every 5 min. Whereas a change in the somatic V_m recordings was observed after IEM1460 application, the fast PF-mediated Ca^{2+} transients did not change, indicating that VGCCs were not directly affected by the blocker. Whereas the Ca^{2+} transient associated with the unpaired CF-EPSP was also not affected, the Ca^{2+} transient associated with the paired CF-EPSP was progressively reduced consistently with the slow mGluR1-mediated Ca^{2+} transient that was extrapolated using a simple fitting of the decay phase of the fast PF-mediated Ca^{2+} transient (Fig. 10*B*). We performed this experiment in $N = 6$ cells, obtaining a significant reduction of the slow mGluR1-mediated Ca^{2+} transient ($p < 0.01$, paired *t* test) 20 min after IEM1460 application, corresponding to a $\Delta F/F_0$ ratio of 0.49 ± 0.16 (Fig. 10*C*). Consistently with this result, the supralinear Ca^{2+} signal, quantified again as the ratio between the paired and the unpaired $\Delta F/F_0$ peaks, significantly ($p < 0.01$, paired *t* test) decreased from 3.37 ± 0.83 to 1.86 ± 0.56 (Fig. 10*D*). We concluded that the mGluR1-dependent supralinear Ca^{2+} signal at *hyp* states is caused by boosting of T-type VGCCs amplified by endogenous buffer saturation produced by the slow mGluR1-dependent PF-mediated Ca^{2+} influx.

Origin of the mGluR1-dependent supralinear Ca^{2+} signals at V_{rest}

The experiments reported in Figures 8 and 10 suggest that the mGluR1-dependent supralinear Ca^{2+} signal also at *rest* state is largely due to saturation of the endogenous buffer, but the results reported in Figure 9 further suggest that an increase in Ca^{2+} influx may contribute in a variable manner. It has been reported that mGluR1 activation shifts the inactivation curve of A-type K^+ channels, boosting the opening of P/Q VGCCs at initial V_m > -65 mV in PNs (Otsu et al., 2014). Thus, consistent with the results of the kinetics analysis reported in Figure 3, an increase in Ca^{2+} influx via P/Q-type VGCCs may contribute to this supralinear Ca^{2+} signal. In contrast with the direct local regulation of T-type VGCCs by mGluR1s (Hildebrand et al., 2009) occurring at *hyp* states, the indirect regulation of P/Q-type VGCCs is produced by a V_m modulation, and therefore, it is not colocalized with mGluR1s. By analyzing cells in which V_{rest} was < -60 mV (i.e., where A-type K^+ channels are not yet fully inactivated), we observed some occasional small supralinear Ca^{2+} signals at sites far away from the PF-activated region at *rest* states. An example of this wide supralinear Ca^{2+} signal is reported in Figures 11*A* and 10*B*. Although this far supralinear Ca^{2+} signal was smaller than the supralinear Ca^{2+} signal colocalized with the PF-mediated signal (Fig. 11*A*), the kinetics were qualitatively similar to those of a "supralinear" Ca^{2+} signal obtained by blocking A-type K^+ channels with the toxin AmmTx3 (Ait Ouares et al., 2019; Zoukimian et al., 2019), as shown in the example in Figure 11*C*.

Finally, in many studies, physiological mGluR1 activation has been mimicked by bath application of the agonist DHPG (for example, see Tempia et al., 2001; Canepari et al., 2001; Maejima et al., 2005; Otsu et al., 2014). We examined this artificial stimulation protocol, which in principle can also produce Ca^{2+} release from internal stores, by applying 100 μM DHPG, using a pipette positioned near the dendrites, with a short (20 ms) pressure ejection as shown in the example in Figure 12*A*. At *hyp* state, DHPG application triggered a slow Ca^{2+} signal, but in contrast to the

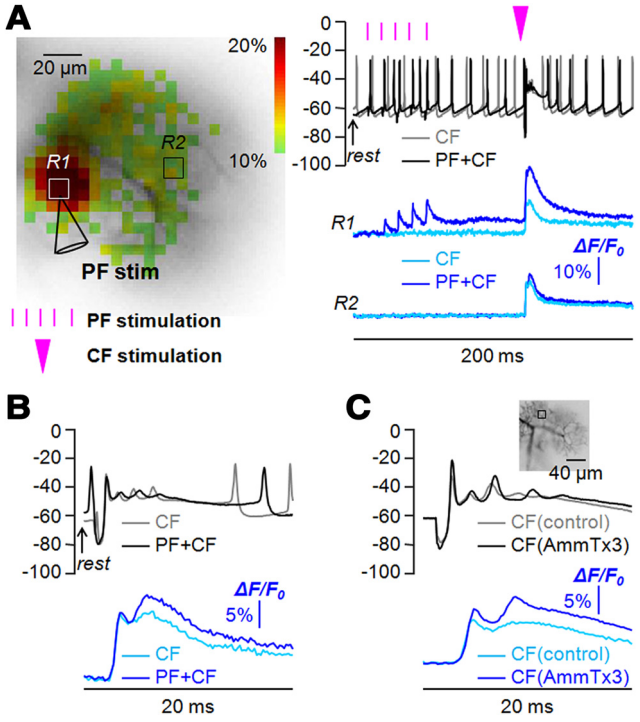

Figure 11. Wide mGluR1-dependent supralinear Ca^{2+} signals at *rest* states. ***A***, Left, Dendrite of PN filled with 2 mM OG5N; position of PF-stimulating electrode and two regions of interest indicated (*R*1 and *R*2). *R*1 is adjacent to the PF-stimulating electrode; *R*2 is ~60 µm away from the PF-stimulating electrode. ***A***, Right, Somatic V_m (top) and dendritic Ca^{2+} signals (bottom) in *R*1 and *R*2 associated with a CF-EPSP unpaired or paired with a PF-EPSP train, with the CF stimulation delayed by 110 ms from the first PF stimulus at *rest* state. ***B***, In a time window of 20 ms, somatic V_m and dendritic Ca^{2+} signals in *R*2 reported in ***A***, exhibiting a supralinear Ca^{2+} transient smaller than that in *R*1. ***C***, Somatic V_m and dendritic Ca^{2+} signal associated with an unpaired CF-EPSP in control condition or after addition of the A-type K^+ channel inhibitor AmmTx3. The two supralinear Ca^{2+} signals reported in ***A*** and ***B*** are qualitatively very similar. All optical signals were from averages of four trials.

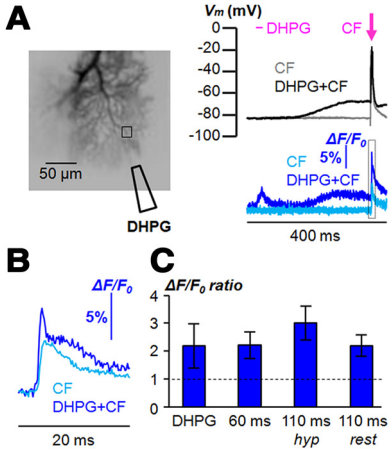

Figure 12. Supralinear Ca^{2+} signals associated with DHPG application. ***A***, Left, Dendrite of PN filled with 2 mM OG5N; a region of interest and the position of a pipette delivering 100 µM DHPG dissolved in external solution are indicated. DHPG application was achieved by applying a 20 ms pulse of pressure using a pressure ejector. ***A***, Right, Somatic V_m (top) and dendritic Ca^{2+} signals (bottom) in the region of interest associated with a CF-EPSP unpaired (light-blue trace) or paired with DHPG application (dark-blue trace); the timing of DHPG application and of CF stimulation is indicated with a purple line and a purple arrow, respectively. A $\Delta F/F_0$ artifact is observable during the short DHPG application. ***B***, In a time window of 20 ms, dendritic Ca^{2+} signals reported in ***A***, exhibiting a supralinear Ca^{2+} transient. ***C***, Left, Mean ± SD (2.20 ± 0.80, $N = 7$ cells) of $\Delta F/F_0$ ratio between the CF-associated signal paired with DHPG application and unpaired. ***C***, Right, Mean ± SD of $\Delta F/F_0$ ratios between CF-associated signals paired with PF stimulation and unpaired; the statistics relative to 60 ms delay between the first PF stimulus and the CF stimulation are the same as reported in Figure 1*D*. The two statistics relative to 110 ms delay between the first PF stimulus and the CF stimulation at *hyp* and *rest* states are the same as reported in Figure 2*D*. The dotted line depicts $\Delta F/F_0$ ratio = 1.

physiological PF stimulation, a corresponding slow V_m depolarization was observed in the soma (Fig. 12*A*). Thus, although a substantial supralinear Ca^{2+} signal associated with DHPG pairing was observed, the kinetics of the Ca^{2+} transient indicate a dominance of Ca^{2+} influx via P/Q-type VGCCs (Fig. 12*B*), consistent with the fact that the initial V_m for the CF-EPSP is ~−60 mV. The size of the supralinear Ca^{2+} signal associated with DHPG application is comparable with those associated with PF stimulation (Fig. 12*C*). Nevertheless, because all of these phenomena are largely due to transient saturation of the endogenous buffer, and the spatial and temporal dynamics of Ca^{2+} influx causing this saturation are different in the different protocols, we conclude that experiments using DHPG application cannot realistically mimic the physiological scenarios associated with mGluR1 activation.

In summary, at the *rest* state, regulation of P/Q-type VGCCs by mGluR1 activation may contribute to the supralinear Ca^{2+} signal, but the localization of this signal, produced by Ca^{2+} influx via these channels, is entirely due to the previous Ca^{2+} entry that saturates the endogenous buffer.

Discussion

Determinants of the different dendritic supralinear Ca^{2+} signals in PNs

In this study, we identified the biophysical determinants of the dendritic supralinear Ca^{2+} signals, observed when a CF-EPSP is preceded by PF activation, that are believed to trigger PF synaptic plasticity (Hartell, 2002; Jörntell and Hansel, 2006; Vogt and Canepari, 2010). In a recent report, we demonstrated that isolated CF-EPSPs essentially trigger Ca^{2+} influx via T-type VGCCs when the initial V_m is <−70 mV and via P/Q-type VGCCs when the initial V_m is >−60 mV (Ait Ouares et al., 2019). In both cases, these signals are spread throughout the dendritic arborization at different extents. Here, we demonstrate that bursts of PF-EPSPs are capable of locally amplifying these two Ca^{2+} signals at the sites of activated PF synapses, driving the CF "error" signal specifically to these inputs (Safo and Regehr, 2008). The biophysical mechanisms that permit these phenomena of amplification are summarized in Figure 13. As shown in Figure 6*B*, a burst of PF-EPSPs locally depolarizes the dendritic area comprising the activated spines. Thus, if a CF-EPSP occurs during this depolarizing phase, the Ca^{2+} influx associated with the CF-EPSP will be principally mediated by P/Q-type VGCCs, independent of the initial V_m. The fast Ca^{2+} influx associated with the PF-mediated depolarization can transiently saturate the endogenous Ca^{2+} buffer, and therefore, a supralinear free Ca^{2+} signal is produced in the dendritic region where V_m is depolarized. It must be pointed out that this type of supralinear Ca^{2+} signal depends on the number and arrangement of activated PFs that determine the spatial pattern of depolarization, but it is not clearly established whether a scenario of "beams" of PF axons activating spines in close proximity occurs *in vivo* (Bower, 2002). During the short PF-mediated depolarization, mGluR1s do not affect the Ca^{2+} transient associated with the CF-EPSP (Fig. 1*D*). After the end of the PF train, V_m is repolarized and mGluR1 effects take action. In this time window, if the repolarized V_m is at the *hyp* state (<−70 mV), the Ca^{2+} influx associated with the CF-EPSP will be prin-

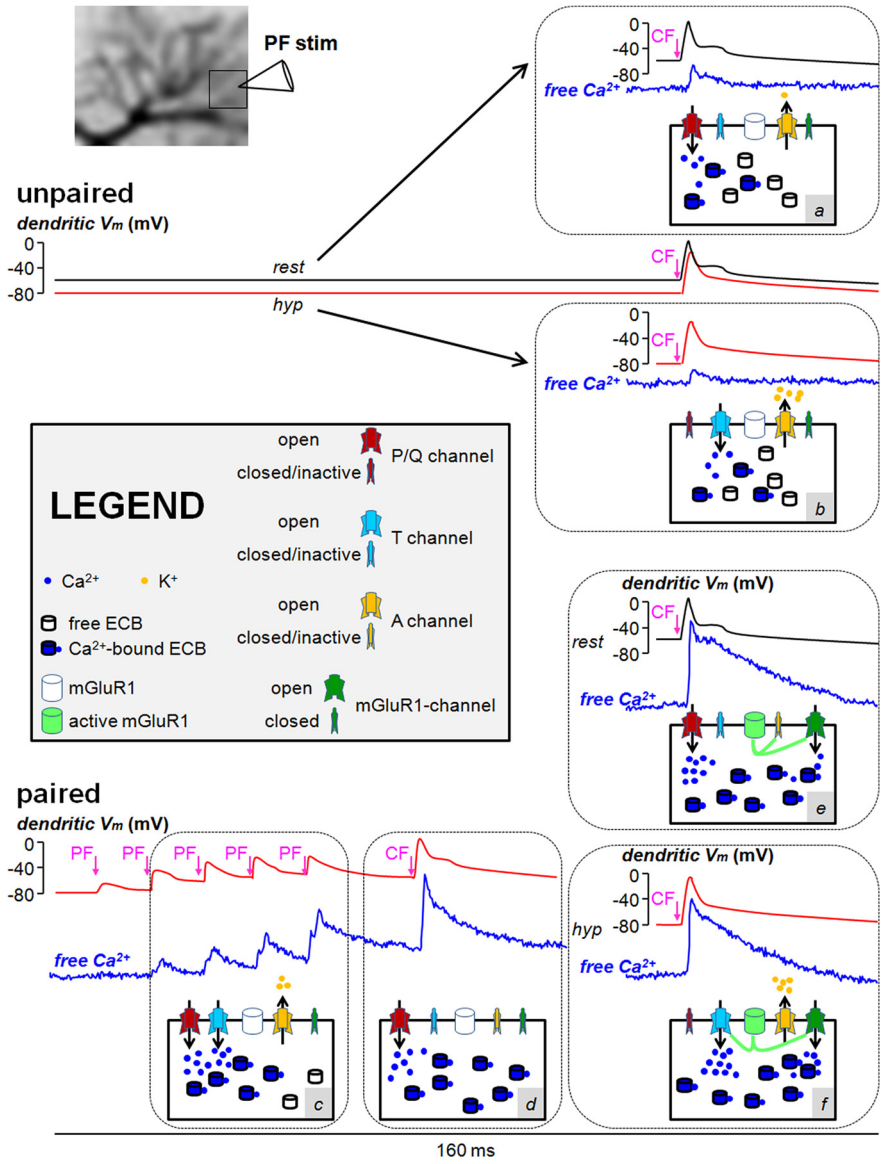

Figure 13. Illustration of the determinants of the different dendritic supralinear Ca^{2+} signals in PNs. Top, A representative PN dendritic region indicating the position of the PF stimulation electrode and a hand-drawn schematic of dendritic V_m associated with an unpaired CF-EPSP and the consequent Ca^{2+} transient at *hyp* and *rest* states. The V_m transient opens principally T and A channels at the *hyp* state (box *b*) and principally P/Q (and possibly A) channels at the *rest* state (box *a*). In both cases, Ca^{2+} entering through VGCCs binds to the endogenous Ca^{2+} buffer (ECB) without saturating it. On the bottom, a hand-drawn schematic of dendritic V_m associated with paired CF-EPSPs and the consequent Ca^{2+} transient. During the PF-EPSPs, Ca^{2+} entering through both VGCC types saturates the ECB (box *c*). At 60 ms delay from the first PF-EPSP, the CF-Ca^{2+} transient principally mediated by P/Q channels produces a supralinear Ca^{2+} increase because the ECB is saturated (box *d*). At 110 ms delay and at *hyp* state, the CF-Ca^{2+} transient produces a supralinear Ca^{2+} increase because T channels are potentiated by active mGluR1s, and the ECB is saturated by Ca^{2+} entering through the mGluR1-activated channel (box *f*). At 110 ms delay and at *rest* state, the CF-Ca^{2+} transient produces a supralinear Ca^{2+} increase because the ECB is saturated by Ca^{2+} entering through the mGluR1-activated channel and possibly because of a larger Ca^{2+} influx via P/Q channels enhanced by stronger inactivation of A channels by mGluR1s (box *e*).

cipally mediated by T-type VGCCs which are potentiated by mGluR1s (Fig. 9). In addition, the slow mGluR1-mediated Ca^{2+} influx is also capable of saturating the endogenous buffer, a mechanism that further amplifies this supralinear free Ca^{2+} signal (Fig. 10). Interestingly, both T channels potentiating and the slow mGluR1-mediated Ca^{2+} influx are triggered by the same mGluR1 pathway (Hildebrand et al., 2009) involving a protein tyrosine phosphatase (Canepari and Ogden, 2003), suggesting that the two factors contributing to this supralinear Ca^{2+} signal colocalize with mGluR1s at a submicron scale. Eventually, if the repolarized V_m is >-65 mV, the Ca^{2+} influx associated with a CF-EPSP will be principally mediated by P/Q-type VGCCs. The Ca^{2+} influx via P/Q-type VGCCs can also be boosted by mGluR1s through inhibition of A-type K^+ channels (Otsu et al., 2014), but with two major differences with respect to the T channel boosting discussed earlier. First, this mechanism is highly variable because, at these initial V_m ranges, A-type K^+ channels are already partially inactivated. Second, the potentiated P/Q channels do not colocalize with the site of activated PFs (Fig. 11*A*,*B*). Thus, the only mechanism providing colocalization in this case is saturation of the endogenous buffer produced by the slow Ca^{2+} influx that is independent of the initial V_m.

Role of the initial V_m and implication for synaptic plasticity

The evidence that mGluR1s locally potentiate a specific Ca^{2+} source (the T-type VGCC) and concomitantly amplify the same signal suggests that the occurrence of a *hyp* state episode is important for synaptic plasticity. Yet, *in vivo* electrode recordings have shown that, in PNs, V_{rest} is similar to that observed in brain slices (Kitamura and Häusser, 2011), indicating that the dendritic V_m is normally not at the *hyp* state. Also, spontaneous bursts of dendritic Ca^{2+} spikes are observed by recording Ca^{2+} and V_m signals simultaneously (Roome and Kuhn, 2018), again indicating that depolarizing transients occur when the dendrite is relatively depolarized. These observations suggest that the *hyp* state might occur exclusively during rare but crucial episodes in which synaptic plasticity may occur. Episodes of *hyp* state can be due, in principle, to synaptic inhibition coactively occurring during activity patterns associated with cerebellar learning (Suvrathan and Raymond, 2018). Indeed, it was recently demonstrated that optogenetic activation of interneurons in the molecular layer strongly affects PF synaptic plasticity and motor learning, as well as CF-mediated signaling (Gaffield et al., 2018; Rowan et al., 2018). Another possibility is that *hyp* state episodes are intrinsically generated in PNs by a "priming" signal that hyperpolarizes the cell, such as by activating a K^+ conductance. Interestingly, in a recent study, it was proposed that PF synaptic depression may physiologically occur when two CF events occur, the first one concomitant with a PF-EPSP burst and the second one after 100 ms (Bouvier et al., 2018). Notably, the concomitant activation of PF and CF inputs hyperpolarizes the PN, as also visible in the examples with 60 ms delay reported in Figures 3*A* and 8*A*.

Role of the mGluR1-activated nonselective cation conductance

An mGluR1-activated nonselective cation conductance, permeable to Ca^{2+}, is the channel that mediates the slow mGluR1 Ca^{2+} influx (Canepari et al., 2001, 2004). This channel has been identified as TRPC3 because, in mutant mice lacking this channel, all signals associated with the mGluR1-activated nonselective cation conductance are absent (Hartmann et al., 2008). This mouse, as well as another mouse model carrying a point mutation in the TRPC3 channel (Becker et al., 2009), exhibit severe changes in behavioral cerebellar functions. More recently, it was shown that mGluR1s can also activate GluD2 delta "orphan" glutamate receptors, raising the question of whether the mGluR1-activated nonselective cation conductance is actually composed of different channels (Ady et al., 2014). Notably, critical mutations of GluRD2 impair synaptic plasticity and motor learning and cerebellar behavioral functions (Hirano, 2006). Regardless of the identity of the channel underlying the slow mGluR1 Ca^{2+} influx, in this study we report a clear role for this conductance. During the time window of mGluR1 action, Ca^{2+} entering the cell after a PF-EPSP burst binds to mobile proteins forming the rich endogenous buffer of PNs (Bastianelli, 2003). Therefore, in this critical time window, the buffer capacity of PN dendrites, which is exceptionally high at rest (Fierro and Llano, 1996), can locally decrease to a level that enables Ca^{2+} influx associated with a CF-EPSP to activate molecular pathways that would not be activated by an unpaired CF-EPSP. The transient saturation of the endogenous buffer has been already identified as a crucial computational element that allows local integration of Ca^{2+} signals (Maeda et al., 1999). However, experimental evidence of endogenous buffer saturation was associated with dendritic depolarization (Canepari and Vogt, 2008), colocalized with activated VGCCs which go beyond the spatial pattern of activated spines. In contrast, endogenous buffer saturation caused by the slow Ca^{2+} influx can be segregated to activated synapses. In general, the spatial pattern of activated spines (Schmidt et al., 2007) and their geometry (Schmidt and Eilers, 2009) are expected to be determinants of endogenous buffer saturation in the case of synaptic Ca^{2+} influx. Finally, endogenous buffer saturation caused by the slow mGluR1 Ca^{2+} influx is likely colocalizing with the potentiated T-type VGCCs when the dendrite is at *hyp* state, because the two mGluR1-mediated mechanisms share the same molecular pathway (Hildebrand et al., 2009).

Perspectives

This study was achieved by monitoring fluorescence simultaneously in large portions of PN dendrites with a spatial resolution of $\sim$10 μM. Thus, the dendritic sites of recording comprise several spines and the parent dendritic segment. A full understanding of the signals in terms of individual spines and dendritic bulks, which is not available in this study, should be achieved in the near future either by reducing the temporal resolution using rapid multisite confocal imaging (Filipis et al., 2018) or by reducing the number of recording spots using two-photon random access microscopy (Otsu et al., 2008). A second question that should be explored in detail is the relation between the initial V_m state and the induction of PF synaptic plasticity. Numerous studies have investigated other parameters as crucial determinants of PF synaptic plasticity, including timing, size of Ca^{2+} signals, spatial arrangements of synaptic inputs, and others (Vogt and Canepari, 2010). In this study, we show that a scenario, in which a specific Ca^{2+} source (the T-type VGCC) is locally boosted and amplified by mGluR1s, occurs only when the initial V_m is hyperpolarized, a phenomenon that can translate into an important information-processing rule associated with cerebellar function.

References

Ady V, Perroy J, Tricoire L, Piochon C, Dadak S, Chen X, Dusart I, Fagni L, Lambolez B, Levenes C (2014) Type 1 metabotropic glutamate receptors (mGlu1) trigger the gating of GluD2 delta glutamate receptors. EMBO Rep 15:103–109.

Ait Ouares K, Jaafari N, Canepari M (2016) A generalised method to estimate the kinetics of fast Ca(2+) currents from Ca(2+) imaging experiments. J Neurosci Methods 268:66–77.

Ait Ouares K, Filipis L, Tzilivaki A, Poirazi P, Canepari M (2019) Two distinct sets of Ca^{2+} and K^+ channels are activated at different membrane potentials by the climbing fiber synaptic potential in Purkinje neuron dendrites. J Neurosci 39:1969–1981.

Ascher P, Nowak L (1987) Electrophysiological studies of NMDA receptors. Trends Neurosci 10:284–288.

Bastianelli E (2003) Distribution of calcium-binding proteins in the cerebellum. Cerebellum 2:242–262.

Becker EB, Oliver PL, Glitsch MD, Banks GT, Achilli F, Hardy A, Nolan PM, Fisher EM, Davies KE (2009) A point mutation in TRPC3 causes abnormal Purkinje cell development and cerebellar ataxia in moonwalker mice. Proc Natl Acad Sci U S A 106:6706–6711.

Bouvier G, Aljadeff J, Clopath C, Bimbard C, Ranft J, Blot A, Nadal JP, Brunel N, Hakim V, Barbour B (2018) Cerebellar learning using perturbations. Elife 7:e31599.

Bower JM (2002) The organization of cerebellar cortical circuitry revisited: implications for function. Ann N Y Acad Sci 978:135–155.

Brenowitz SD, Regehr WG (2005) Associative short-term synaptic plasticity mediated by endocannabinoids. Neuron 45:419–431.

Canepari M, Mammano F (1999) Imaging neuronal calcium fluorescence at high spatio-temporal resolution. J Neurosci Methods 87:1–11.

Canepari M, Ogden D (2003) Evidence for protein tyrosine phosphatase, tyrosine kinase, G-protein regulation of the parallel fiber metabotropic slow EPSC of rat cerebellar Purkinje neurons. J Neurosci 23:4066–4071.

Canepari M, Ogden D (2006) Kinetic, pharmacological and activity-dependent separation of two Ca^{2+} signalling pathways mediated by type 1 metabotropic glutamate receptors in rat Purkinje neurones. J Physiol 573:65–82.

Canepari M, Vogt KE (2008) Dendritic spike saturation of endogenous calcium buffer and induction of postsynaptic cerebellar LTP. PLoS One 3:e4011.

Canepari M, Papageorgiou G, Corrie JE, Watkins C, Ogden D (2001) The conductance underlying the parallel fibre slow EPSP in rat cerebellar Purkinje neurones studied with photolytic release of l-glutamate. J Physiol 533:765–772.

Canepari M, Auger C, Ogden D (2004) Ca^{2+} ion permeability and single-channel properties of the metabotropic slow EPSC of rat Purkinje neurons. J Neurosci 24:3563–3573.

Canepari M, Willadt S, Zecevic D, Vogt KE (2010) Imaging inhibitory synaptic potentials using voltage sensitive dyes. Biophys J 98:2032–2040.

Debanne D (1996) Associative synaptic plasticity in hippocampus and visual cortex: cellular mechanisms and functional implications. Rev Neurosci 7:29–46.

Fierro L, Llano I (1996) High endogenous calcium buffering in Purkinje cells from rat cerebellar slices. J Physiol 496:617–625.

Filipis L, Ait Ouares K, Moreau P, Tanese D, Zampini V, Latini A, Bleau C, Bleau C, Graham J, Canepari M (2018) A novel multisite confocal system for rapid Ca^{2+} imaging from submicron structures in brain slices. J Biophotonics 11:e201700197.

Finch EA, Augustine GJ (1998) Local calcium signalling by inositol-1,4,5-trisphosphate in Purkinje cell dendrites. Nature 396:753–756.

Gaffield MA, Rowan MJM, Amat SB, Hirai H, Christie JM (2018) Inhibition gates supralinear Ca^{2+} signaling in Purkinje cell dendrites during practiced movements. Elife 7:e36246.

Hartell NA (1994) Induction of cerebellar long-term depression requires activation of glutamate metabotropic receptors. Neuroreport 14:913–916.

Hartell NA (2002) Parallel fiber plasticity. Cerebellum 1:3–18.

Hartmann J, Dragicevic E, Adelsberger H, Henning HA, Sumser M, Abramowitz J, Blum R, Dietrich A, Freichel M, Flockerzi V, Birnbaumer

L, Konnerth A (2008) TRPC3 channels are required for synaptic transmission and motor coordination. Neuron 59:392–398.
Hildebrand ME, Isope P, Miyazaki T, Nakaya T, Garcia E, Feltz A, Schneider T, Hescheler J, Kano M, Sakimura K, Watanabe M, Dieudonné S, Snutch TP (2009) Functional coupling between mGluR1 and Cav3.1 T-type calcium channels contributes to parallel fiber-induced fast calcium signaling within Purkinje cell dendritic spines. J Neurosci 29:9668–9682.
Hirano T (2006) Cerebellar regulation mechanisms learned from studies on GluRdelta2. Mol Neurobiol 33:1–16.
Hyrc KL, Bownik JM, Goldberg MP (2000) Ionic selectivity of low-affinity ratiometric calcium indicators: mag-fura-2, Fura-2FF and BTC. Cell Calcium 27:75–86.
Isope P, Hildebrand ME, Snutch TP (2012) Contributions of T-type voltage-gated calcium channels to postsynaptic calcium signaling within Purkinje neurons. Cerebellum 11:651–665.
Ito M (2001) Cerebellar long-term depression: characterization, signal transduction, functional roles. Physiol Rev 81:1143–1195.
Jaafari N, Canepari M (2016) Functional coupling of diverse voltage-gated Ca(2+) channels underlies high fidelity of fast dendritic Ca(2+) signals during burst firing. J Physiol 594:967–983.
Jaafari N, De Waard M, Canepari M (2014) Imaging fast calcium currents beyond the limitations of electrode techniques. Biophys J 107:1280–1288.
Jaafari N, Marret E, Canepari M (2015) Using simultaneous voltage and calcium imaging to study fast Ca^{2+} channels. Neurophotonics 2:021010.
Jörntell H, Hansel C (2006) Synaptic memories upside down: bidirectional plasticity at cerebellar parallel fiber-Purkinje cell synapses. Neuron 52:227–238.
Kano M, Garaschuk O, Verkhratsky A, Konnerth A (1995) Ryanodine receptor-mediated intracellular calcium release in rat cerebellar Purkinje neurones. J Physiol 487:1–16.
Kim SJ, Jin Y, Kim J, Shin JH, Worley PF, Linden DJ (2008) Transient upregulation of postsynaptic IP3-gated ca release underlies short-term potentiation of metabotropic glutamate receptor 1 signaling in cerebellar Purkinje cells. J Neurosci 28:4350–4355.
Kitamura K, Häusser M (2011) Dendritic calcium signaling triggered by spontaneous and sensory-evoked climbing fiber input to cerebellar Purkinje cells in vivo. J Neurosci 31:10847–10858.
Knöpfel T, Vranesic I, Staub C, Gähwiler BH (1991) Climbing fibre responses in olivo-cerebellar slice cultures. II. Dynamics of cytosolic calcium in Purkinje cells. Eur J Neurosci 3:343–348.
Kosaka T, Kosaka K, Nakayama T, Hunziker W, Heizmann CW (1993) Axons and axon terminals of cerebellar Purkinje cells and basket cells have higher levels of parvalbumin immunoreactivity than somata and dendrites: quantitative analysis by immunogold labeling. Exp Brain Res 93:483–491.
Maeda H, Ellis-Davies GC, Ito K, Miyashita Y, Kasai H (1999) Supralinear Ca^{2+} signaling by cooperative and mobile Ca^{2+} buffering in Purkinje neurons. Neuron 24:989–1002.
Maejima T, Oka S, Hashimotodani Y, Ohno-Shosaku T, Aiba A, Wu D, Waku K, Sugiura T, Kano M (2005) Synaptically driven endocannabinoid release requires Ca^{2+}-assisted metabotropic glutamate receptor subtype 1 to phospholipase Cbeta4 signaling cascade in the cerebellum. J Neurosci 25:6826–6835.
Miyakawa H, Lev-Ram V, Lasser-Ross N, Ross WN (1992) Calcium transients evoked by climbing fiber and parallel fiber synaptic inputs in guinea pig cerebellar Purkinje neurons. J Neurophysiol 68:1178–1189.
Nägerl UV, Novo D, Mody I, Vergara JL (2000) Binding kinetics of calbindin-D(28k) determined by flash photolysis of caged Ca(2+). Biophys J 79:3009–3018.
Otsu Y, Bormuth V, Wong J, Mathieu B, Dugué GP, Feltz A, Dieudonné S (2008) Optical monitoring of neuronal activity at high frame rate with a digital random-access multiphoton (RAMP) microscope. J Neurosci Methods 173:259–270.
Otsu Y, Marcaggi P, Feltz A, Isope P, Kollo M, Nusser Z, Mathieu B, Kano M, Tsujita M, Sakimura K, Dieudonné S (2014) Activity-dependent gating of calcium spikes by A-type K+ channels controls climbing fiber signaling in Purkinje cell dendrites. Neuron 84:137–151.
Roome CJ, Kuhn B (2018) Simultaneous dendritic voltage and calcium imaging and somatic recording from Purkinje neurons in awake mice. Nat Commun 9:3388.
Rowan MJM, Bonnan A, Zhang K, Amat SB, Kikuchi C, Taniguchi H, Augustine GJ, Christie JM (2018) Graded control of climbing-fiber-mediated plasticity and learning by inhibition in the cerebellum. Neuron 99:999–1015.e6.
Safo PK, Regehr WG (2005) Endocannabinoids control the induction of cerebellar LTD. Neuron 48:647–659.
Safo P, Regehr WG (2008) Timing dependence of the induction of cerebellar LTD. Neuropharmacology 54:213–218.
Savitzky A, Golay JE (1964) Smoothing and differentiation of data by simplified least squares procedures. Anal Chem 36:1627–1639.
Schmidt H, Eilers J (2009) Spine neck geometry determines spino-dendritic cross-talk in the presence of mobile endogenous calcium binding proteins. J Comput Neurosci 27:229–243.
Schmidt H, Kunerth S, Wilms C, Strotmann R, Eilers J (2007) Spino-dendritic cross-talk in rodent Purkinje neurons mediated by endogenous Ca^{2+}-binding proteins. J Physiol 581:619–629.
Suvrathan A, Raymond JL (2018) Depressed by learning-heterogeneity of the plasticity rules at parallel fiber synapses onto Purkinje cells. Cerebellum 17:747–755.
Takechi H, Eilers J, Konnerth A (1998) A new class of synaptic response involving calcium release in dendritic spines. Nature 396:757–760.
Tempia F, Alojado ME, Strata P, Knöpfel T (2001) Characterization of the mGluR(1)-mediated electrical and calcium signaling in Purkinje cells of mouse cerebellar slices. J Neurophysiol 86:1389–1397.
Vogt KE, Canepari M (2010) On the induction of postsynaptic granule cell-Purkinje neuron LTP and LTD. Cerebellum 9:284–290.
Vogt KE, Gerharz S, Graham J, Canepari M (2011a) High-resolution simultaneous voltage and Ca^{2+} imaging. J Physiol 589:489–494.
Vogt KE, Gerharz S, Graham J, Canepari M (2011b) Combining membrane potential imaging with L-glutamate or GABA photorelease. PLoS One 6:e24911.
Wang SS, Denk W, Häusser M (2000) Coincidence detection in single dendritic spines mediated by calcium release. Nat Neurosci 3:1266–1273.
Zoukimian C, Meudal H, De Waard S, Ouares K, Nicolas S, Canepari M, Béroud R, Landon C, De Waard M, Boturyn D (2019) Synthesis by native chemical ligation and characterization of the scorpion toxin AmmTx3. Bioorg Med Chem 27:247–253.